DEVELOPMENT OF A FLUORESCENCE RESONANCE ENERGY TRANSFER OPTICAL NANOSCALE BIOSENSOR BASED ON A LIQUID-CORE WAVEGUIDE PLATFORM

A Thesis
presented to
the Faculty of the Graduate School
at the University of Missouri-Columbia

In Partial Fulfillment
of the Requirements for the Degree

Master of Science

---

by

R CODY STRINGER

Dr. Sheila Grant, Thesis Supervisor

AUGUST 2007

The undersigned, appointed by the dean of the Graduate School, have examined the thesis entitled

DEVELOPMENT OF A FLUORESCENCE RESONANCE ENERGY TRANSFER OPTICAL NANOSCALE BIOSENSOR BASED ON A LIQUID-CORE WAVEGUIDE PLATFORM

presented by R Cody Stringer,

a candidate for the degree of Master of Science

and hereby certify that, in their opinion, it is worthy of acceptance.

Dr. Sheila Grant, Biological Engineering Dept.

Dr. Susan Schommer, Veterinary Pathobiology Dept.

Dr. Xudong Fan, Biological Engineering Dept.

ACKNOWLEDGEMENTS

I would like to sincerely thank Dr. Sheila Grant for her guidance and patience with my research. She has shown tireless confidence and faith in my abilities, allowing me to accomplish things that I would not have thought possible. Time and time again, she has pushed me forward, giving me fortitude, opportunities, advice, or just a friendly word.

I would also like to thank Dr. Susan Schommer for the materials and counsel that she has given throughout my work, and Dr. Xudong Fan for challenging me at every turn, making me a more thorough and encompassing researcher.

Additionally, I would like to thank Darcy Lichlyter and Daniel Hoehn for their help in the laboratory. Their assistance was invaluable for the progress of this research project.

TABLE OF CONTENTS

LIST OF FIGURES

DEVELOPMENT OF A FLUORESCENCE RESONANCE ENERGY TRANSFER OPTICAL NANOSCALE BIOSENSOR BASED ON A LIQUID-CORE WAVEGUIDE PLATFORM

R Cody Stringer

Dr. Sheila Grant, Thesis Supervisor

ABSTRACT

In order to produce a more versatile, adaptable, and effective method for detection of biological analytes, a self-contained and robust fluorescent optical biosensor architecture utilizing fluorescence resonance energy transfer (FRET) is proposed. This biosensor architecture is then applied to a highly adept liquid-core waveguide platform. FRET is a distance-dependent signal transduction method that occurs between two fluorescent molecules, termed the donor and acceptor. When the donor and acceptor are brought within close proximity, a quantifiable nonradiative energy exchange takes place. In order to launch FRET, a donor-labeled Protein A molecule is bound to an acceptor-labeled capture antibody. When exposed to antigen, the antibody-antigen binding event initiates a conformational change within the structure of the antibody, and thereby induces a measurable change in energy transfer from the donor to the acceptor by altering the distance between the FRET pair. Additionally, effects of quantum dots and gold nanoparticles utilized within the FRET system are studied. The resulting system is then optimized and tested in a liquid-core waveguide platform that is able to retrieve sensitive and accurate measurements. In the current study, the biosensor was used to detect Porcine Reproductive and Respiratory Syndrome virus and human cardiac Troponin I, showing ample sensitivity and a high degree of specificity, as well as rapid response.

CHAPTER 1. LITERATURE REVIEW

1.1 Optical Biosensors

A sensor can be defined simply as a device that responds to a physical property in order to measure or detect it. Because the field of sensors is extremely broad, it can be divided into three primary classes: physical, chemical, and biological. Physical sensors measure physical quantities, such as temperature, pressure, or weight, while chemical sensors use chemical reactions to respond to a particular substance, or rather, a particular analyte. Biological sensors, or biosensors, are often considered a subclass of chemical sensors, though they have the distinction of exclusively using biological elements for analyte response. The basic elements of a biosensor device, as shown in Figure 1, include the sample to be tested for presence or concentration of the analyte of interest, the biological recognition element that responds in some fashion to the analyte, the transducer that acts to convert the recognition element response to a useable signal, and finally, the detector or signal processor, which uses the transduction signal to produce appropriate and meaningful output information. The analyte of interest determines what type of transducer a biosensor is to employ. The type of transducer, in turn, determines the appropriate detector or signal processor. There are four fundamental types of transduction methods that biosensors utilize, and these are electrochemical, optical, piezo-electric, and thermal[1].

Figure 1. Schematic of basic biosensor elements

There are also various structures that can be used as the biological recognition element. These structures can be divided into catalyst-based systems and affinity-based systems. The catalyst-based systems utilize enzymes, while affinity-based systems use antibodies and receptors. Because of their catalytic activity, enzymes are able to convert a biological macromolecule into a different, product macromolecule while remaining unchanged itself, leaving it free to continue to convert other macromolecules. The affinity-based systems, on the other hand, use binding reactions, which are often irreversible without the use of strong solvents that damage and reduce the binding capabilities of the recognition element. Oftentimes, the antibodies and receptors used in affinity-based systems are more robust and easy to use and maintain, and can also be produced for a huge array of different analytes[2].

Because of the use of biological elements, biosensors have the distinct advantage of being extremely versatile. They are capable of detecting a single analyte with very high specificity, meaning that the sensor responds only to one substance without being affected by others. However, they are also capable of detecting a host of related analytes simultaneously for a more encompassing method of detection. Biosensors are also capable of high levels of sensitivity, where sensitivity describes the magnitude of the change in output signal of the sensor when exposed to analyte. Because of high affinities or strengths of many biological reactions, biosensors are also well suited for relatively rapid response times, often obtaining an output signal within seconds of analyte exposure.

On the other hand, the inherent use of biological systems limits applications and longevity of biosensors. In particular, these systems are damaged in harsh conditions, such as extreme pH levels or temperatures, and must therefore be confined to specific

environments. They are also commonly perishable and are only able to retain their properties for a limited time. In general, biosensors can be designed with these principles in mind so that, for all practical purposes, they may be neglected.

Optical biosensors utilize the principles of optics for generation of a suitable output signal, in essence by altering the light characteristics of the transducer. When the biological recognition element interacts with the analyte of interest, a change in optical properties such as absorption, fluorescence, or refractive index occurs. With the appropriate signal processor, such changes in optical properties can be converted to meaningful information about the analyte[3].

There exist two classes of optical biosensors and these are direct and indirect. Indirect optical biosensors use macromolecules that are labeled or tagged in some way. Typical methods include radioactive, fluorescent, and enzyme labeling. These methods usually provide very strong, highly sensitive output signals and are the preferred method when practical. Direct optical biosensors function without the use of a label and often rely on changes in refractive index or absorption of the biosensor system. In this manner, direct methods are applicable for situations when labeling of biological compounds is impractical[2].

Due to high sensitivity and ease of labeling, fluorescence-based indirect optical biosensors are a preferred method for a variety of applications. The high sensitivity of these systems is due to the ability of current detection methods to measure minute amounts of fluorescent material. They are also capable of obtaining information when incorporated into many different types of optical biosensor configurations, including

those that examine protein-protein interactions and protein conformational changes for affinity-based biosensor systems[4].

Fluorescence is a process in which light energy is absorbed and subsequently reemitted. This process is best depicted in the Jablonski diagram shown in Figure 2, which illustrates the molecular absorption of a photon, causing an electron be excited, jumping from the ground state to an excited energy state. The electron then relaxes to the lowest unoccupied molecular orbital of the excited energy state band. At this point, the electron can return to the ground state either with the emission of a photon, which results in fluorescence, or without the emission of a photon. Alternatively, intersystem crossing can occur, resulting in an event known as phosphorescence, though this process is of little importance to the current research[5].

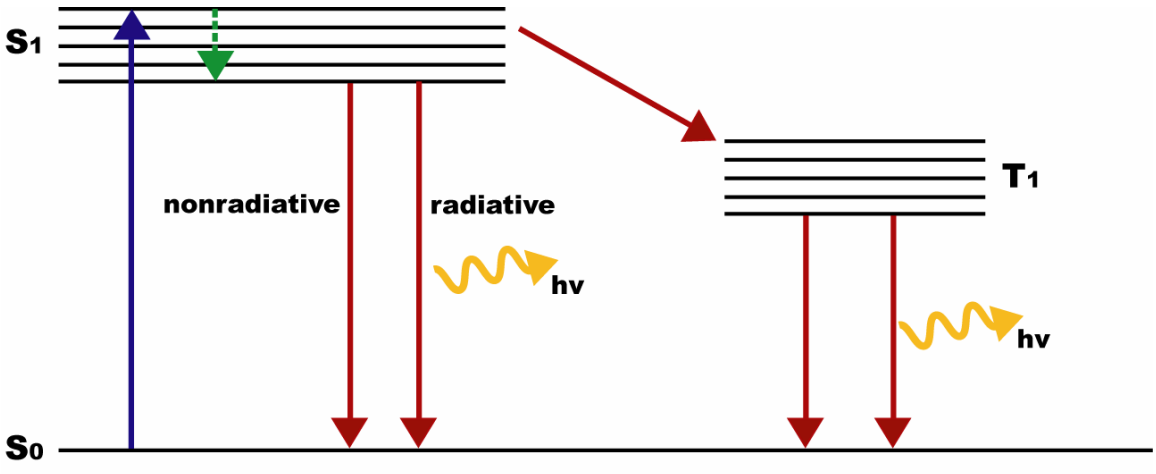

Figure 2. Jablonski diagram depicting the process of fluorescence

When light is reemitted during the process of fluorescence, it does so from a lower energy state than that with which it was originally excited due to the electron's relaxation to the lowest unoccupied molecular orbital. This results in the fluorescent light having a lower energy and, therefore, a longer wavelength than the absorbed incident

light. This phenomenon is known as Stokes shift, and the consequence is a fluorescent substance having a photon absorption peak at a shorter wavelength than its mirror image emission peak, with the Stokes shift, or spectral distance, between the two peaks being dependent on the optical properties of the substance[5].

Fluorescent molecules are readily labeled to biological molecules for use in fluorescent optical biosensors. Such systems have been shown to effectively detect a variety of analytes, including glucose[6], an array of biohazardous agents[7], and DNA[8], just to name a few.

1.2 Fluorescence Resonance Energy Transfer

Although the direct measurement of fluorescence is a powerful tool in optical biosensor applications, fluorescence resonance energy transfer (FRET) takes advantage of certain principles of fluorescence to further increase the sensitivity of such systems. FRET is a chemical transduction method that takes place between two fluorescent species, with one termed the donor and the other the acceptor. Each fluorescent molecule acts as an oscillating dipole, and the donor and acceptor fluorescent molecules are able to undergo long-range dipole – dipole interactions. In order for FRET to occur, the donor and acceptor must be within close proximity, as FRET is only effective over a distance range of 10-100 Å, the fluorescence emission peak of the donor must overlap sufficiently with the absorption peak of the acceptor, and the dipoles of the fluorescent molecules must be oriented appropriately. When these requirements are met, energy is transferred from the donor to the acceptor nonradiatively and resonantly, meaning that the process

does not involve the absorption or emission of photons. This process is illustrated in Figure 3.

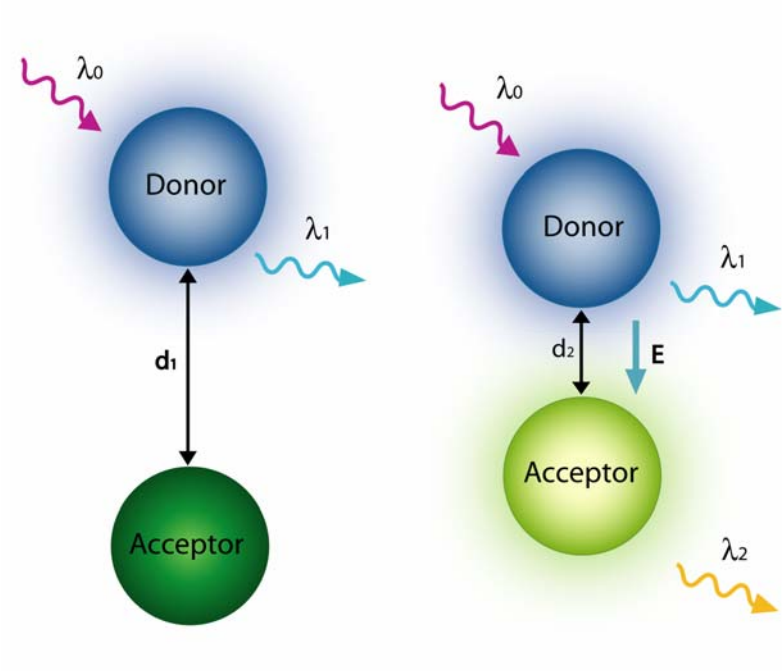

Figure 3. Illustration of FRET occurring between two fluorescent molecules

The amount of energy transferred from the donor to the acceptor during the FRET process is distance-dependent, and can be described by Eq. 1, the energy transfer efficiency equation.

$$E = \frac{R_0^6}{R_0^6 + r^6} \tag{1}$$

The energy transfer efficiency (E), then, is described in terms of the Förster distance (R_0) and the spatial distance between the donor and acceptor (r). The Förster

distance is an intrinsic property of the donor and acceptor FRET pair, and is defined as the distance at which energy transfer efficiency is 50%.

Because the process of FRET is distance-dependent, it is often considered to be a highly sensitive "molecular ruler." In order to exploit FRET for distance measurements, the change in energy transfer efficiency must be dramatic with respect to distance between the donor and acceptor. By examining the energy transfer efficiency equation plotted over an arbitrary distance, as shown in Figure 4, it can be observed that the distances in which the largest change in E takes place is over the range $0.5R_0 < r < 1.5R_0$. These distances are commonly within the range of 20-60 Å, and because this corresponds to the scale of many biological macromolecule diameters, it has been used extensively in the field of molecular biology[5,9]. In the field of biosensors, FRET has been utilized for an array of applications, with include the study of protein-protein association events[10], virus detection[11], and bacteria detection[12].

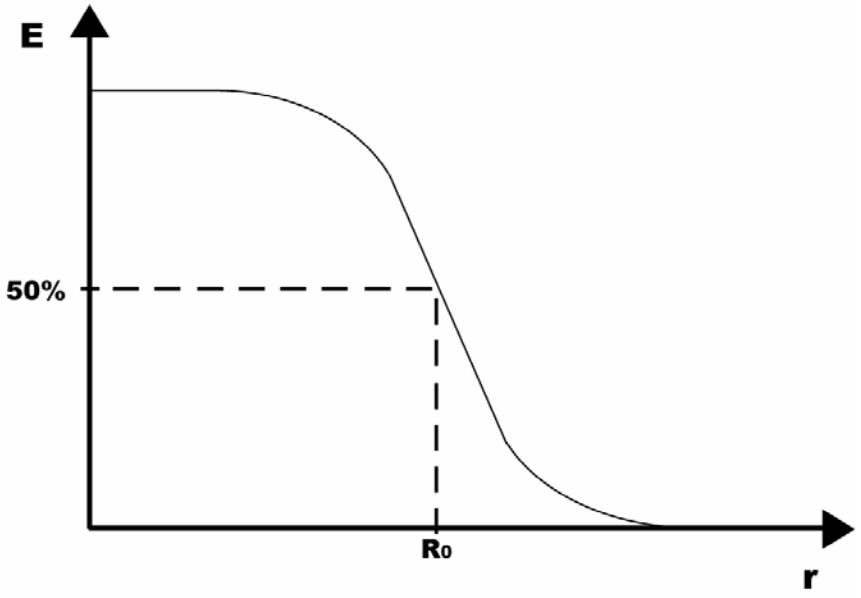

Figure 4. Graph of FRET energy transfer efficiency versus distance between donor and acceptor

1.3 Nanophotonic Particles

One major advance in the field of optics technology is the advent of nanophotonics. Nanophotonics deals with the interaction of light and matter on a nanometer, or one-billionth of a meter, sized scale. Because the scale with which nanophotonic interactions occur is usually below that of the wavelength of light, nanophotonic interactions involve alterations in the properties of the electrons within the system. The two types of nanophotonic particles used in this study are metallic nanoparticles and quantum dots. Both of these nano-scale particles are able to interact with light, but each does so with very different electronic interactions[13].

Metallic nanoparticles are particles 1-100 nm in diameter that possess the ability to absorb light very effectively within a particular wavelength range. This occurs due to a phenomenon known as the plasmon resonance effect. Metallic materials carry the unique property of having free and highly mobile surface electrons. When light at a particular frequency, or wavelength, interacts with a metallic nanoparticle, the electrons at the nanoparticle surface become polarized. The oscillating electromagnetic field of the incident light then causes dipolar oscillation of the electrons, and a plasmon resonance effect is produced, with the effect of effectively absorbing the incident light[13,14].

When the incident light is provided by a fluorescent molecule acting as a donor, with the metallic nanoparticle acting as an acceptor, the fluorescence of the donor will be quenched. This process, however, occurs due to both radiative plasmon resonance effects as well as nonradiative FRET effects, which increases the quenching efficiency of the metallic nanoparticle[15]. These metallic nanoparticle acceptor systems have been utilized in biosensor applications for the detection of insulin[16], neurotoxins[17], and DNA[18].

Quantum dots, on the other hand, are composed of inorganic semiconducting material, such as CdSe, CdS, or ZnS. In a bulk semiconducting material, the minimum energy required to cause an electron to jump from the valence band to the conduction band, referred to as the band gap, is constant and is considered a property of the material. Along with the energy band gap, however, there is also a spatial distance that the electron must travel to reach the conduction band, which is called the exciton Bohr radius. For quantum dots, the size of the semiconducting material approaches the Bohr radius, or 2-8 nm in diameter. This process, called quantum confinement, produces two important electronic properties different from that of the bulk material. Firstly, the conduction band becomes separated into discrete sub-bands, resulting in emission of light from the material when an electron returns to the valence band from the conduction band. Secondly, the band gap of the material is no longer constant, and instead increases as the size of the quantum dot decreases. The size-dependent property of the band gap, then, causes a size-tunable property of the wavelength of emitted light. As the diameter of the quantum dot decreases, so does the wavelength of light that will be emitted when an electron returns to the valence band[13,19].

Other than size-tunability of the fluorescence emission wavelength, quantum dots have several advantageous optical properties. Firstly, the quantum dot can be capped by coating it with several atomic layers of a semiconductor material with a wider band gap, which gives the quantum dot greater photostability and a higher quantum yield[20]. In addition, quantum dots have extremely broad absorption spectra and narrow emission peaks, with wide effective Stokes shifts[21]. A broad absorption spectrum allows the quantum dot donor to be excited at low, often ultraviolet, wavelengths. In FRET

applications, this allows the quantum dot to act as a donor molecule, which can be excited with a light source so as to minimize direct acceptor excitation. The result is a FRET system that is entirely resistant to photobleaching. Such FRET-based biosensor systems with quantum dot donors have been used for detection of maltose[22], cortisol[23], and an array of proteases[24].

1.4 Antibody Mobility

Applications in which FRET has proven to be a useful tool include examination of protein-protein interactions, protein conformational changes, and DNA hybridization. However, the study of protein conformational changes in biosensor applications is quite limited. Due to their high level of structural flexibility, immunoglobulin G (IgG) antibodies are well suited for such a purpose.

IgG antibodies are Y-shaped proteins that are produced by the immune system for identification and removal of foreign substances. The antibody structure, as shown in Figure 5, consists of an F_C, or constant portion, and two F_{AB}, or variable portions. The F_C section of the antibody is essentially conserved for all antibodies, while the F_{AB} segments contain hypervariable regions that constitute the antigen binding site. The antigen binding sites are present at the ends of each F_{AB} segment and are responsible for the high specificity and binding affinity for the antigen with which they recognize. Furthermore, the F_C segment is connected to the two F_{AB} arms by means of a hinge region that gives the F_{AB} regions flexibility with respect to the F_C region, as well as each other[25,26].

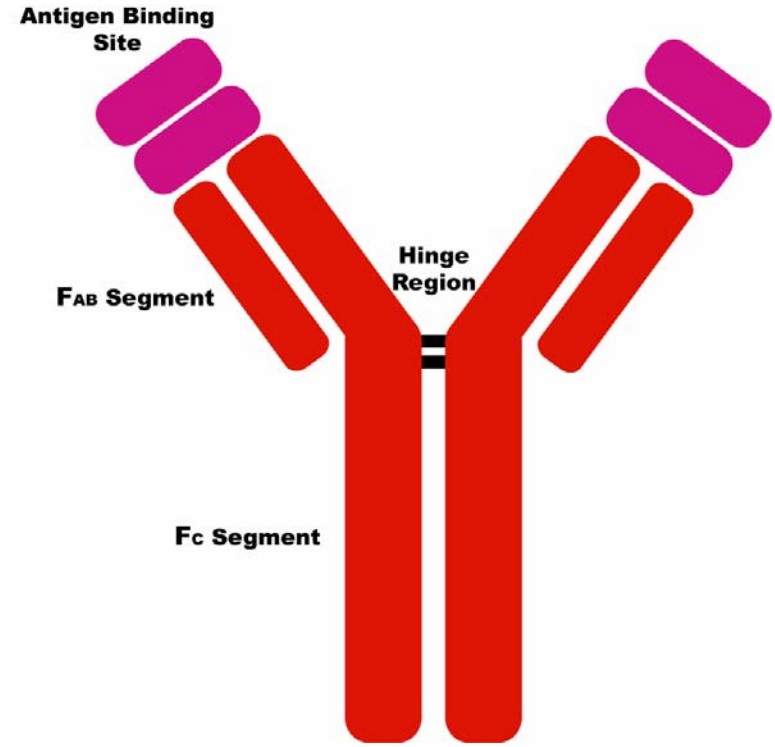

Figure 5. Illustration of IgG antibody structure

Although the two F_{AB} arms are highly flexible, they are not freely moving structures. Instead, intrinsic potential energy within the molecule results in a bias towards a certain conformation. The potential energy also results in anti-cooperativity effects between the two F_{AB} arms, causing them to move away from each other when the antigen-antibody encounter complex forms. This increases ability of the antibody to bind two antigens simultaneously by reducing the steric hindrance of the bound antigen to the available antigen binding site, or to bind one antigen with increased strength for larger antigen molecules with multiple epitopes[27]. The result is a prominent and dramatic conformational change that takes place within the antibody structure upon antigen binding. By utilizing FRET to examine these changes, biosensors have been developed that have successfully been used to detect human IgG antibodies[28] and viral particles[29].

1.5 Total Internal Reflection and Liquid-Core Waveguide Principles

The principle of total internal reflection (TIR) is an optical technique that allows light to be confined to a particular medium. When light travels through a medium with a refractive index n_1, and interacts at an incident angle of θ_1 with another medium with a refractive index n_2, the light will undergo reflection and/or refraction, with the angle of refracted light being θ_2. This interaction is depicted in Figure 6.

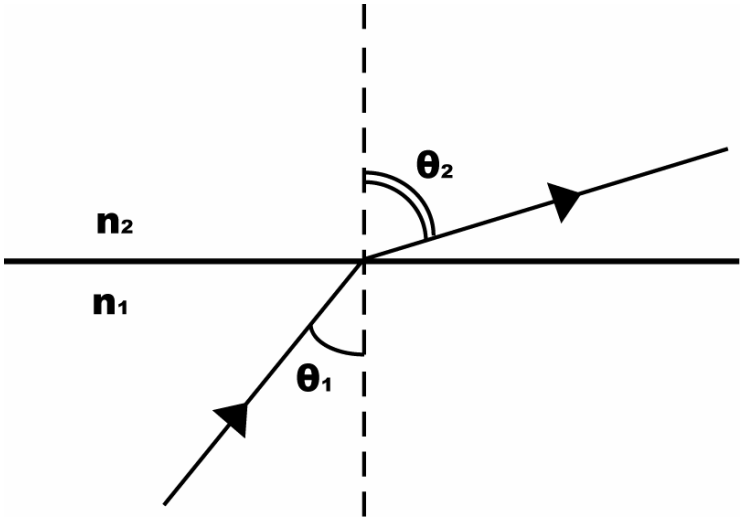

Figure 6. Depiction of the process of total internal reflection

Snell's law, as shown in Eq. 2 below, describes this interaction.

$$n_1 \sin\theta_1 = n_2 \sin\theta_2 \tag{2}$$

When the refractive index of the medium with which light interacts, n_2, is less than the refractive index of the medium in which it is traveling, n_1, and if the incident angle θ_1 is sufficiently large, TIR will occur and the light will only undergo reflection.

The angle above which TIR occurs is referred to as the critical angle, θ_C. By setting θ_2 equal to 90 degrees, Eq. 2 can be rearranged so that the critical angle equation is found[30].

$$\theta_C = \arcsin\left(\frac{n_2}{n_1}\right) \tag{3}$$

This principle is the basis of optical waveguide devices, such as optical fibers, which use TIR to both manipulate and guide light along a designated path. Light enters the higher refractive index medium, termed the core, and is then confined to the core by the lower refractive index medium, termed the cladding[31].

When the medium in which light is to be confined is a fluid, it can be approximated to have optical properties equal to that of water (refractive index $n \sim 1.33$), and materials that are capable of internalizing the fluid while having a refractive index lower than that of water are limited. One such material, Teflon AF, is both suitable for confining light within a fluid core and is also commercially available. Dupont's Teflon AF, a copolymer of 1, 3-dioxole, 4, 5-difluoro-2, 2-bis(trifluoromethyl) and tetrafluoroethene, is available in two grades: 2400 (refractive index $n \sim 1.29$) and 1600 (refractive index $n \sim 1.31$)[32]. The polymer not only exhibits refractive index lower than that of water, but is also transparent and readily molded into various shapes for the effective confinement of a fluid core.

For use in biosensor applications, Teflon AF-based liquid-core waveguide (LCW) devices have been utilized for an array of applications. The fluoropolymer itself may be molded into tubing, allowing nearly complete transparency as well as gas permeability.

Such tubing has been applied to sensing applications that include Raman spectroscopy[33-35], trace gas sensing[36], and luminescence[37] and fluorescence[38] detection. Alternatively, Teflon AF may be found in the form of a resin, and can be applied to the interior of glass capillary tubing and dried to form a Teflon AF-clad tube. These capillary-based LCWs have proven highly efficient at guiding light emitted by fluorescent dyes within the core[39,40]. By the same token, a thin layer of Teflon AF resin may be applied to substrates in order to coat micro channels[41], though the biosensor applications of this method remain largely unrealized.

For fluorescent-based applications, the use of liquid-core waveguides has distinct advantages. Most notably, the waveguides are capable of simultaneously confining the fluidic solution while guiding the light emitted from the fluorescent molecules in the solution to each terminus of the waveguide. Also, the incident light used to excite the fluorescent solution may be configured in a number of ways, depending upon the specific requirements of the application. For the purposes of fluorescent biosensor applications, transverse excitation is often the most effective method. By angling the excitation light perpendicular to the waveguide, it is able to pass through the transparent Teflon AF cladding into the fluid core where it excites the fluorescent solution, then continues through the adjacent cladding and into the external medium. In this way, minimal excitation light is transmitted through the fluid core to the waveguide termini, as it simply passes transversely through it. This has the benefit of reducing excitation light interference by acting as an excitation filter. Additionally, once the emitted fluorescent light reaches the waveguide terminus, it can either be directly measured or coupled into another waveguide, such as an optical fiber, for remote measurements[42].

CHAPTER 2. INTRODUCTION TO RESEARCH

2.1 Significance of Research

Two different analytes were studied during the course of this research. The first analyte was Porcine Reproductive and Respiratory Syndrome virus (PRRSV). Porcine Reproductive and Respiratory Syndrome Virus (PRRSV) is an extremely contagious enveloped, single-stranded positive-sense RNA virus. According to Hanada et al.[43], its evolution rate is one of the highest reported among RNA viruses since it was transmitted to swine circa 1980. Clinical symptoms of the virus include reproductive failure, post-weaning pneumonia, growth reduction, and increased mortality, with persistent infection having been reported to last up to 3 months[44]. Once the virus has infected a population, the most attractive method of disease elimination is diagnosis and removal of infected animals, as compared to depopulation/repopulation techniques, and expeditious diagnosis of infected animals is key to properly controlling the spread of the virus[45]. Currently, methods for PRRSV detection include reverse transcription-polymerase chain reaction (RT-PCR), indirect fluorescence antibody test (IFAT), and enzyme linked immunosorbent assay (ELISA)[46]. These methods, however, are costly, time-consuming, and must be carried out in a laboratory. The result of these disadvantages is the continued spread of the virus while diagnostic tests are being conducted, as well as removal of individuals that are no longer infected.

The second analyte studied was human cardiac Troponin I (cTnI). Cardiac Troponin exists as a complex of three subunits: Troponin I, T, and C. Because the amino acid sequences of cardiac muscle Troponin T and I differ from the sequences found in

skeletal muscle, the T and I subunits correspond only to cardiac muscle. Upon myocardial damage, the myocyte membrane loses integrity as necrosis occurs, and cardiac Troponin is released into the bloodstream, where it persists for several hours[47]. In the clinical setting, this property allows effective diagnosis of acute myocardial infarction or other damage with the use of commercially available assay techniques.

Although the currently available assay methods are highly effective at detecting the presence of Troponin T or I, and often achieve extremely low limits of detection in the range of 0.01-0.1 ng/ml[48], they still suffer from a large incidence of false positives[47]. Other diagnostic methods are then required to substantiate positive results of a cardiac Troponin assay.

2.2 Research Objectives

The objective of this research was to develop a versatile optical biosensor by investigating novel nano-sensing mechanisms and sensing platforms such as LCWs. The basic biosensor architecture utilizes the highly distance-sensitive FRET method to detect conformational changes in antibody structure upon the formation of the antibody-antigen encounter complex. Additionally, nanophotonic particles, namely metallic nanoparticles and quantum dots, are introduced into the FRET system for increased efficiency sensitivity.

The proposed biosensor has the distinct advantage of being capable of being employed in-solution or adapted to be immobilized onto a substrate. Because immobilizing the biological recognition element on a substrate often causes a loss of activity or hindrance of available binding sites, it is often unfavorable to do so. However,

the working principles of nearly all biosensor designs rely on a substrate for proper functioning. The ability of a biosensor to function in-solution creates a much more flexible sensor design. Also, due to the in-solution nature of the biosensor, it can be effectively deployed within a LCW system. This allows the biosensor to benefit from the advantages of the LCW platforms, further increasing the efficacy of the optical biosensor.

In order to develop the stated biosensor, the following objectives must be consecutively completed:

- Investigate and fabricate basic nano-biosensor architectures, using FRET to measure conformational changes in antibody structure upon antigen binding.
- Examine the in-solution biosensor response by exposing the fabricated biosensor architectures to analyte of interest and measuring the change in fluorescent energy transfer.
- Use the biosensor analyte response to develop and optimize the biosensor.
- Apply the optimized biosensor architecture to a suitable LCW platform.
- Determine the efficacy of the biosensor when applied to the LCW by again measuring the in-solution biosensor analyte response.

The final goal of this research was to design and develop an effective diagnostic tool for the detection of a host of analytes. Ideally, the biosensor could be integrated into a comprehensive and field deployable lab-on-a-chip device capable of autonomously taking measurements after introduction of the test sample.

CHAPTER 3. IN-SOLUTION OPTICAL BIOSENSOR ARCHITECTURE DEVELOPMENT

3.1 Overview

The envisioned biosensor architectures consist of an antibody-based biological macromolecule complex. The complex is comprised of the analyte-specific antibody bound to Protein A, a protein capable of binding to the F_C portion of IgG antibodies. By labeling the IgG antibody with a traditional organic fluorescent dye, and the Protein A molecule with a nanophotonic particle, the complex is able to undergo FRET. Upon antigen binding, a conformational change takes place in the antibody structure, altering the distance between the FRET pair. This causes a change in the energy transfer efficiency of the FRET pair, producing a measurable change in the fluorescence spectrum of the biosensor. The two architectures studied utilized either a quantum dot or a gold nanoparticle as the nanophotonic element in the FRET pair, and the analyte used to test the efficacy of the optical biosensor was PRRSV.

3.2 Materials and Methods

3.2.1 Fluorescent Labeling

Protein A labeled with 20 nm colloidal gold nanoparticles, unlabeled Protein A, bovine serum albumin (BSA), Tris buffered saline, and phosphate buffered saline (PBS) were purchased from Sigma-Aldrich (St. Louis, MO). 1-Ethyl-3-[3-dimethylaminopropyl]carbodiimide hydrochloride (EDC) and *N*-hydroxysulfosuccinimide (sulfo-NHS) were purchased from Pierce (Rockford, Il). The

organic fluorophore used was Alexa Fluor 546, which was purchased from Invitrogen (Carlsbad, CA) and conjugated to an SDOW17 anti-PRRSV monoclonal antibody purchased from Rural Technologies, Inc (Brookings, SD). This antibody was chosen based on its ample binding affinity to a highly conserved epitope on the PRRSV nucleocapsid. Conjugation and purification were conducted according to the protocol provided with the Alexa-fluor 546 dye. Briefly, 25 µl monoclonal antibody, 10 µl sodium bicarbonate, and 65 µl PBS were combined and added to the Alexa-fluor 546 reactive fluorescent dye vial. The reaction mixture was incubated for 1 hour at room temperature. Next, spin columns were prepared with 30,000 D molecular weight size-exclusion resin and the PBS solvent was removed from the resin by centrifuging at 1100 x g for 3 minutes to create a size-exclusion gel inside the spin column. The gel bed was loaded with the Alexa-fluor 546-monoclonal antibody reaction mixture and centrifuged at 1100 x g for 5 minutes. The solution passing through the gel bed during centrifugation was the labeled antibody. This solution was collected and the spin column containing the entrapped free Alexa-fluor 546 dye was discarded.

Protein A was labeled with Catskill green quantum dots, which were purchased from Evident Technologies (Troy, NY) and conjugated as described in the provided protocol. Briefly, 20 µl distilled water, 40 µl 10X PBS, 200 µl carboxyl functionalized quantum dots (0.25 mg/ml), 10 µl EDC (200 mg/ml), and 100 µl sulfo-NHS (0.15 mg/ml) were combined and incubated with constant gentle mixing at room temperature for approximately 1 hour. Next, the reaction mixture was desalted by filtering with a Pall Nanosep 100 K spin filtration column (East Hills, NY) centrifuged at 10,500 rpm for 15 minutes. The volume was brought to 500 µl with PBS and 294.5 µl Protein (1.0 mg/ml)

was added for a 4:1 Protein A to quantum dot molar ratio. This reaction mixture was incubated for approximately 1 hour with constant gentle mixing, and subsequently quenched by addition of 88.3 µl Tris buffered saline. The solution was then once again filtered with a 100 K spin filtration column. The resulting solution, quantum dot-labeled Protein A, was brought to a total volume of 400 µl with PBS.

The Catskill green quantum dot was chosen as the donor because its emission peak wavelength, which occurs at approximately 544 nm, directly overlaps the absorption peak wavelength of the Alexa-fluor acceptor, which occurs at approximately 546 nm. By the same token, 20 nm colloidal gold was utilized as the acceptor because of its high degree of absorption at a wavelength of 546 nm.

3.2.2 Degree of Labeling

Determination of the degree of labeling is an important aspect of optical biosensor development. Essentially, the degree of labeling is a measurement of the number of fluorescent molecules per biological macromolecule. Using the degree of labeling, the number of donor fluorescent molecules and the number of acceptor fluorescent molecules can be maintained constantly over each optical sensor solution, even when the degree of labeling of the reagent solution changes between labelings. This is important so that reagents are not wasted in investigating, through trial and error, the optimum molar ratio of donor to acceptor each time a new labeling is performed. Instead, the proper molar ratio of donor to acceptor is found once, and as the reagents are consumed and new samples are labeled, the proper concentrations of reagent are calculated using the degree of labeling.

For the Alexa-fluor 546 labeled antibody, the degree of labeling is found using the protocol provided with the Alexa-fluor labeling kit. Briefly, optical absorbance measurements are conducted with a Beckman DU 520 UV/Vis spectrophotometer (Fullerton, CA) at wavelengths of 280 nm and 558 nm. These values are then applied to Equation 4 to find the antibody concentration.

$$[antibody(M)] = \frac{A_{280} - (A_{558} \times 0.12)}{203{,}000} \tag{4}$$

In Equation 4, A_{280} and A_{558} are the measured absorbance at 280 nm and 558 nm, respectively, 0.12 represents a correction factor to account for absorption of the dye at 280 nm, and 203,000 $cm^{-1}M^{-1}$ is the molar extinction coefficient of the IgG antibody. Using the calculated antibody concentration, the degree of labeling is then calculated using Equation 5.

$$\frac{fluorophores}{protein} = \frac{A_{558}}{104{,}000 \times [antibody(M)]} \tag{5}$$

In this equation, 104,000 $cm^{-1}M^{-1}$ is the molar extinction coefficient of Alexa-fluor 546 at a wavelength of 558 nm. This value is the experimentally obtained degree of labeling of Alexa-fluor 546 onto the analyte-specific antibody.

The degree of labeling for the quantum dot is difficult to measure due to the large overlap in absorbance of the quantum dot with the protein to which it is labeled. In this case, it is assumed that the concentration of Protein A for each reagent labeling is consistent enough that variations can be neglected. This assumption is only valid because it is the concentration of quantum dot, and not Protein A, that is of importance. To find the molar concentration of quantum dot in the reagent solution, the absorbance of the

quantum dot at its first excitation peak is measured, and the concentration of quantum dot is then calculated using the Lambert-Beer law, shown in Equation 6 below.

$$A_{525} = \varepsilon \cdot l \cdot c \tag{6}$$

In this equation, A_{525} is the measured absorbance at 525 nm, ε is the molar extinction coefficient of the Catskill green quantum dot, which is approximately equal to 72,000 $cm^{-1}M^{-1}$, l is the pathlength, which is equal to 1 cm, and c is the molar concentration of the quantum dot in the solution of labeled Protein A.

The degree of labeling of gold nanoparticles is not measured. The Protein A labeled with gold nanoparticles is purchased in a bulk solution and is therefore considered constant

3.2.3 Biosensor Fabrication

Once the reagents were labeled with the appropriate fluorescent molecules, the sensor architecture was fabricated. By combining the two reagents, the sensor underwent self-assembly as Protein A bound to the F_c portion of the SDOW17 antibody. PRRSV was isolated from the Ingelvac PRRS vaccine purchased from Boehringer Ingelheim Vetmedica, Inc (St. Joseph, MO), and the viral capsid was lysed via introduction of 0.2% (v/v) Triton X-100 purchased from Sigma-Aldrich (St. Louis, MO). Proper molar ratios of Alexa-fluor 546-labeled SDOW17 antibody to quantum dot- or gold nanoparticle-labeled Protein A were chosen based on maximum sensor response to a quantity of PRRSV much greater than that required to theoretically saturate the biosensor. This theoretical saturation value was found by calculating the total number of antigen binding

sites in the sensor solution. Since each anti-PRRSV antibody has two available antigen binding sites, the number of antibodies in solution multiplied by two is equal to the maximum number of antibody-antigen encounter complexes that can occur. However, actual saturation occurs at a lower concentration due to steric hindrance of available binding sites by bound antigen on the same antibody.

Since the degree of labeling of the gold nanoparticle-based biosensor is unable to be found, so too is the optimum molar ratio of donor to acceptor. Instead, the variation in the number of gold nanoparticles is neglected and the concentration is adjusted according only to the degree of labeling of the Alexa-fluor 546-labeled antibody. For the quantum dot-based sensor, however, the most effective ratio must allow both the donor and acceptor emission peaks to remain distinct and quantifiable. By qualitatively examining the emission peaks of the FRET pair in the biosensor solution, it was determined that a 4:1 Alexa-fluor 546 to quantum dot ratio provided the emission spectrum with noticeable peaks and measurable energy transfer changes. This FRET pair ratio was used for all subsequent experiments. Both sensor architectures were fabricated by incubating a bulk solution of labeled antibody and labeled Protein A overnight at 4°C, and was then divided into 8.0 µl aliquots for use.

3.2.4 Measurement of Biosensor Response

The response of the fabricated biosensor was examined by exposing each sensor aliquot to various concentrations of PRRSV, ranging from 0-60 particles/µl. Specificity was confirmed by exposing each sample to either PRRSV or a nonspecific protein, BSA. All antigen exposure times were approximately 1 hour at room temperature. PBS was

added to each sample for a total sample volume of 1 ml and the samples were scanned in a Jobin Yvon Fluoromax-3 spectrofluorometer (Stanmore, UK).

Biosensor response was measured by observing the intensity of the fluorescence peaks obtained from the spectrofluorometer scans. For the gold nanoparticle-based sensor, the intensity of the Alexa-fluor 546 emission peak was used as a relative quantification of the fluorescence quenching effects of the colloidal gold. For the quantum dot-based sensor, the intensity of both the quantum dot and the Alexa-fluor 546 fluorescence emission peaks were utilized. By dividing the quantum dot emission by the Alexa-fluor 546 emission, a ratio of donor fluorescence to acceptor fluorescence (D/A) was obtained. The D/A value acted as a ratiometric quantification of energy transmitted from the quantum dot to the Alexa-fluor 546 dye. Optical biosensor response is a consequence of a greater number of conformational changes taking place in the sensor solution upon antigen binding. The conformational changes alter the distance between the donor and acceptor, causing a measurable change in the resonance energy transfer that occurs between the fluorescent molecules. The result is a derived measurement of antigen concentration in the solution based on changes in the observed spectral properties.

3.2.5 Enzyme-linked Immunosorbent Assay Protocol

The SDOW17 antibody was biotinylated using the biotin labeling kit purchased from Invitrogen (Carlsbad, CA). PRRSV and Protein A coating solutions were prepared in dilutions of 1:100 and 1:1000 in 0.1 M sodium bicarbonate, and biotinylated SDOW17 antibody was diluted to a final concentration of 3 μg/ml in sodium bicarbonate. A

volume of 100 µl of the coating solutions were added to an Immulon 4HBX 96-well immunoassay plate purchased from Thermo Scientific (Waltham, MA), and incubated overnight at 4^{o}C. Negative controls were provided by adding sodium bicarbonate coating buffer only to the appropriate wells, and positive controls were provided by adding the biotinylated SDOW17 in coating buffer to the appropriate wells. The wells were then washed twice with 200 µl PBS/Tween solution, blocked with a 3% BSA in PBS solution, and washed again. Next, 100 µl biotinylated SDOW17 antibody was added to each well and incubated for approximately 2 hours at room temperature. Each well was washed six times with PBS/Tween.

Avidin-peroxidase and 2,2′-Azino-bis(3-ethylbenzothiazoline-6-sulfonic acid) (ABTS) enhancer were purchased from Sigma-Aldrich (St. Louis). According to manufacturer recommendations, avidin-peroxidase was prepared in a 1:400 dilution in blocking buffer, added to each well, and incubated approximately 30 minutes. The wells were then washed eight times with PBS/Tween. Finally, ABTS enhancer was added to each well and allowed to develop for approximately 15 minutes. The optical absorbance at a wavelength of 415 nm was read for each well using a Bio-Rad Model 680 microplate reader (Hercules, CA).

3.3 Results and Discussion

3.3.1 PRRSV Concentration Response

Biosensor response to various concentrations of PRRSV antigen is shown in Figure 7. PRRSV concentrations ranged from 0-60 particles/µl. As PRRSV binds to the Alexa-fluor 546-labeled SDOW17 antibody, a conformational change results and the

Alexa-fluor 546 fluorophore moves away from the nanophotonic molecule, causing a decrease in energy transfer from the donor to the acceptor. As a greater number of PRRSV particles are introduced to the biosensor solution, a greater number of biosensor complexes are affected, causing a greater change in biosensor value. For the gold nanoparticle-based sensor, this causes a decrease in the quenching effect of the colloidal gold as greater concentrations of PRRSV are added to the sensor solution, as shown in Figure 7(a). For the quantum dot-based sensor, less energy is being transferred from the quantum dot to the Alexa-fluor 546, causing an increase in quantum dot fluorescence with a corresponding decrease in Alexa-fluor 546 fluorescence, as shown in Figure 7(b).

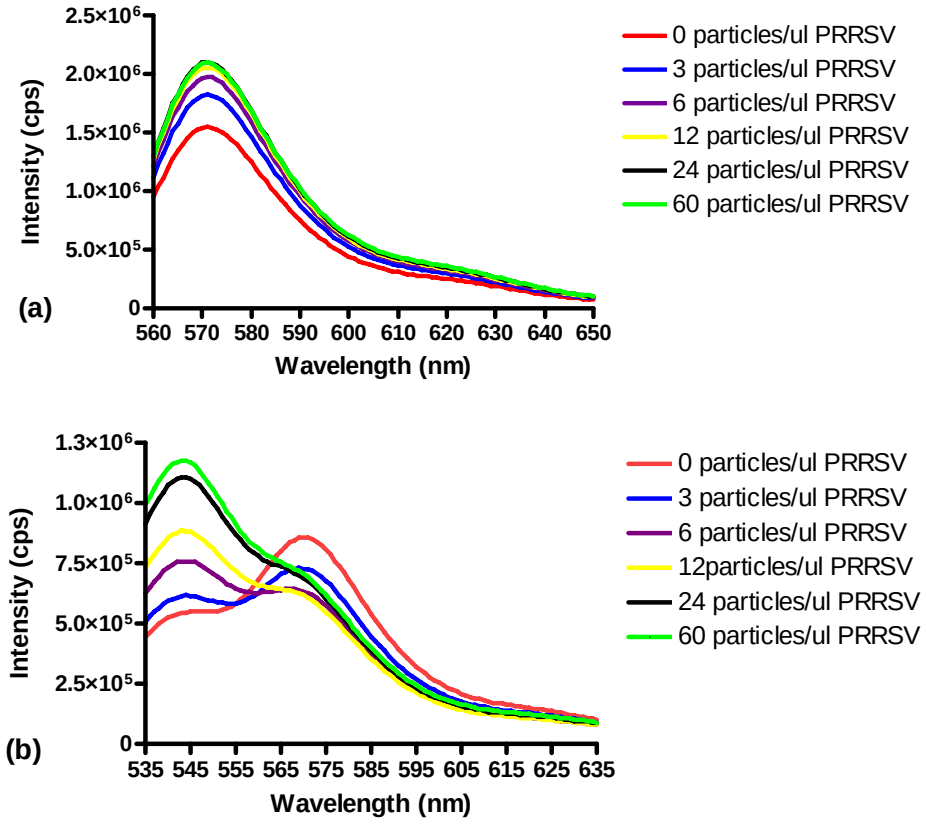

Figure 7. Fluorescence spectra for (a) gold nanoparticle biosensor and (b) quantum dot biosensor with PRRSV concentrations ranging from 0-60 particles/µl

By plotting the biosensor response values (fluorescence intensity for gold nanoparticle sensor and D/A value for quantum dot sensor) for various concentrations of PRRSV, concentration curves are obtained for gold nanoparticle biosensor and quantum dot biosensor, as shown in Figure 8a and Figure 8b respectively.

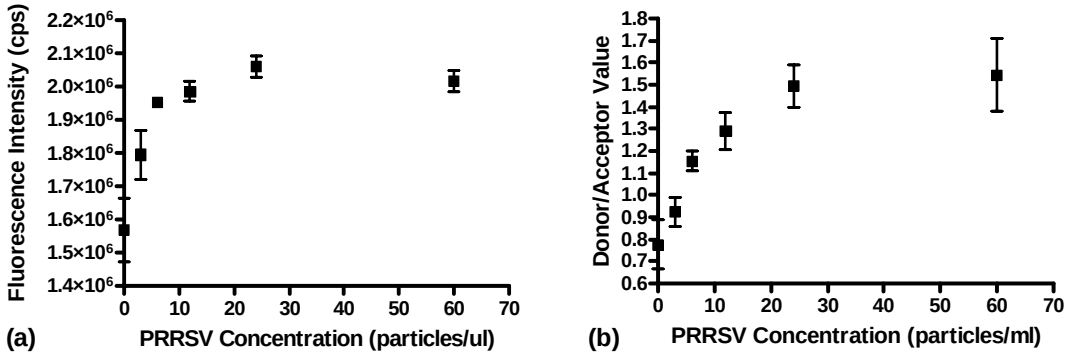

Figure 8. Dose response curves for (a) gold nanoparticle biosensor and (b) quantum dot biosensor

Both the gold nanoparticle-based sensor and the quantum dot-based sensor concentration curves show a characteristic linear trend with increasing PRRSV concentration, followed by a saturation region at high antigen concentration. This saturation region was between 20 and 30 particles/µl for both sensor architectures. For the gold nanoparticle-based sensor, an R^2 value of 0.8144 was achieved, with a detection limit of 1741 particles/ml. For the quantum dot-based sensor, an R^2 value of 0.7835 was achieved, with a detection limit of 1409 particles/ml. Neither the predictive values nor detection limits are currently fitting enough to ensure accurate and consistent diagnostic values, but are indicative of the feasibility of the sensor for PRRSV detection. Because of the small volumes of sensor solutions utilized in these experiments, the solution was diluted in PBS for a total volume of 1 ml in order to be effectively scanned in the spectrofluorometer, leading to slight dilution variation between samples. Such dilution

effects decrease the sensitivity of the biosensor system, and it is believed that miniaturizing the system so that smaller volumes may be measured will decrease error caused by dilution variation and greatly enhance the detection limit of the biosensor. As an added benefit, miniaturization of the biosensor will also allow it to be developed as a field-deployable device.

3.3.2 Biosensor Specificity

By exposing both the gold nanoparticle- and quantum dot-based sensors to large concentrations of either PRRSV or BSA, the specificity of the biosensor was attained. In Figure 9(a), the gold nanoparticle-based sensor produced a clear response to PRRSV, while producing negligible response to the BSA nonspecific antigen, demonstrating that this sensor is indeed highly specific to PRRSV. The quantum dot-based sensor in Figure 9(b), however, produced noticeable response to both PRRSV and BSA.

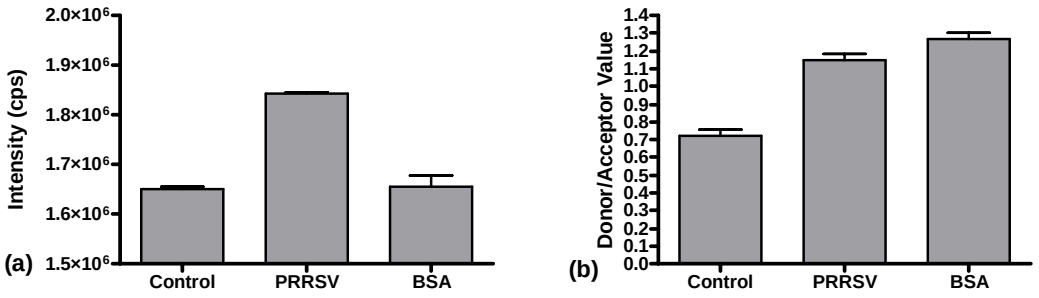

Figure 9. Specificity of sensor response for (a) gold nanoparticle biosensor and (b) quantum dot biosensor is illustrated by comparing the response to PRRSV as compared to a nonspecific antigen, BSA

Upon closer examination, this nonspecific response to BSA is not produced due to a decrease in FRET, which is characterized by an increase in donor fluorescence

accompanied by a decrease in acceptor fluorescence. By inspecting the fluorescence spectra, it was instead discovered that as the concentration of BSA increased, there was an increase in the quantum dot donor fluorescence, but this was accompanied by a proportional increase in Alexa-fluor 546 acceptor fluorescence. This illustrated that, rather than specific BSA binding to the capture antibody causing a FRET decrease, the BSA was causing an increase in the apparent quantum yield of the quantum dot. As the quantum dot fluorescence increases, the acceptor fluorescence also increases, but by a proportionately smaller degree. The result is an increasing D/A value that yields a nonspecific biosensor response.

3.3.3 Investigation of Lack of PRRSV Antibody-Antigen Binding

After completion of in-solution sensor feasibility studies, the PRRSV antigen solution was consumed and a new stock solution was prepared by again lysing the viral capsid with 2% (v/v) Triton X-100. The results of subsequent biosensor experiments showed negligible response to antigen, and it was believed that antibody-antigen binding was no longer occurring.

To determine if the most recently prepared PRRSV antigen was properly binding to the IgG antibody, an enzyme-linked immunosorbent assay (ELISA) was conducted. With the ELISA technique, the antigen was adsorbed onto a substrate and the antibody, labeled with a tracer, was allowed to bind to the immobilized antigen. Using a colorimetric reaction, binding between antigen and antibody can be determined. Additionally, unlabeled Protein A and gold nanoparticle-labeled Protein A were also adsorbed onto the substrate to determine whether the biosensor was assembling properly.

When the ELISA is complete, a presence of a colorimetric reaction compared to the negative control indicates positive binding between the two species, either antibody-Protein A or antibody-PRRSV. Once the ELISA had been allowed to develop, an image of the well plate was taken and is shown in Figure 10.

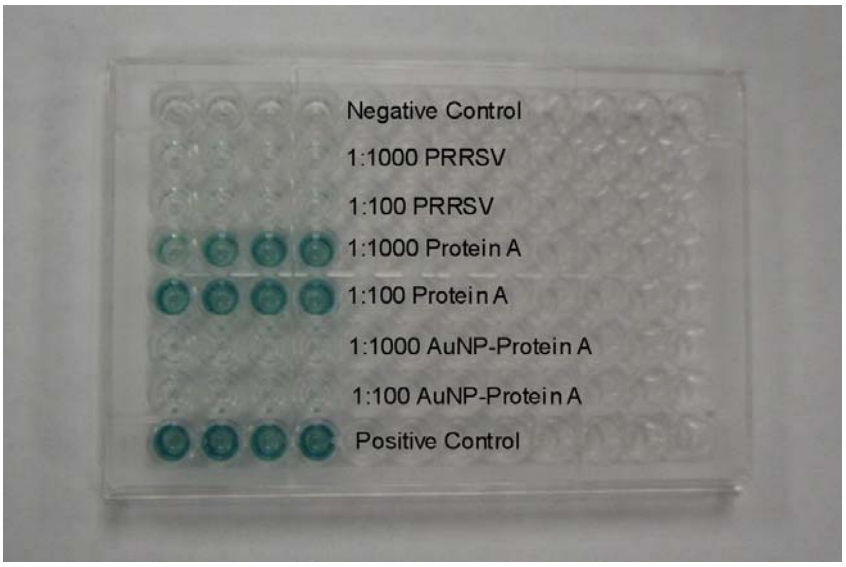

Figure 10. Image of complete PRRSV biosensor ELISA well plate

The optical absorbance at a wavelength of 415 nm was then found for each well. Each row of the well plate contains four repetitions, and so the wells in each row were averaged to account for slight variations. These values are shown graphically in Figure 11.

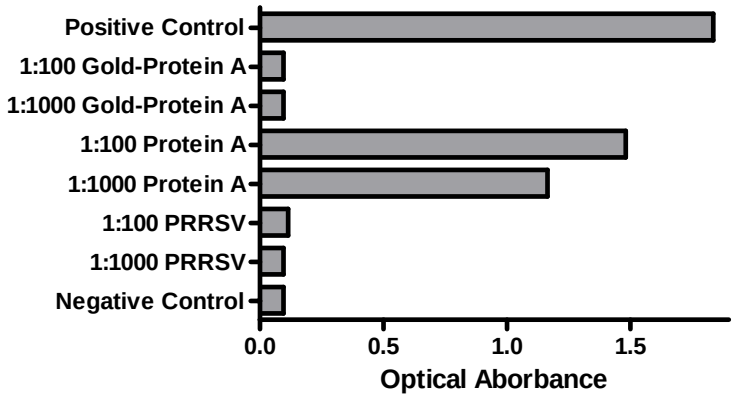

Figure 11. Optical absorbance values for PRRSV biosensor ELISA

The results of the PRRSV biosensor ELISA indicate that binding is occurring between the SDOW17 IgG antibody and the unlabeled Protein A. However, binding did not occur between the antibody and the PRRSV antigen or the gold nanoparticle-labeled Protein A. Insufficient binding between the IgG antibody and the PRRSV antigen explains why negligible biosensor response was observed after antigen preparation, however the reasons behind the lack of binding are unclear. A total of eight ELISAs were conducted, examining the effect of alternative anti-PRRSV antibodies and PRRSV isolates. Antibody-antigen binding was negative in each case.

On the other hand, the lack of binding between the IgG antibody and the gold nanoparticle-labeled Protein A can be attributed to steric hindrance by the gold nanoparticles on the surface of the Protein A molecule. It is likely that this only occurs when the Protein A is immobilized onto a substrate due to the enhanced antibody binding hindrance of the substrate and adjacent Protein A molecules.

3.4 Conclusions

The results of these experiments indicate that, although further development is necessary, the proposed optical biosensors are feasible methods for PRRSV detection. As compared to the gold nanoparticle-based sensor, the quantum dot sensor is less susceptible to dilution effects and other errors that may be introduced during sensor fabrication due to the ratiometric nature of data acquisition. Additionally, the quantum dot is unsusceptible to photobleaching, which creates a highly stable FRET system. In this manner, the quantum dot sensor is highly robust and more suitable for accurate PRRSV detection, though nonspecific response of the sensor must first be corrected before applications in PRRSV detection are possible.

The nonspecific response of the quantum dot biosensor can likely be attributed to the instability of the quantum dot's coating layer in water. Quantum dots are intrinsically non-water soluble, and must hence be coated or functionalized with a water stabilization layer, such as a phospholipid micelle, or a polymer or silica shell[20]. It is assumed that the introduction and nonspecific adsorption of a protein to the quantum dot surface alters the water stabilization layer and increases the apparent quantum yield, though the processes behind this phenomenon are currently unclear and continued studies are required.

Additionally, ELISA results illustrate that the biosensor is being fabricated properly, although binding is no longer occurring between the anti-PRRSV antibody and the PRRSV antigen. For subsequent biosensor experiments, an alternative antigen was utilized.

CHAPTER 4. DEPLOYMENT OF OPTICAL BIOSENSOR ONTO LIQUID-CORE WAVEGUIDE PLATFORM

4.1 Overview

Due to the intrinsic benefits of the quantum dot-based biosensor architecture, it was chosen as the optimal sensor complex. Although a large degree of nonspecific response was observed, advantages such as ratiometric nature of measurements and increased photostability make the quantum dot-based sensor much more suitable for biosensor applications than the gold nanoparticle architecture. It was also theorized that because the increasing quantum yield effects of the quantum dot were likely caused by the aqueous environment in which it was being used, decreasing the volume of PBS used in sensor experiments would diminish the occurrence of nonspecific antigen response.

The optimized quantum dot biosensor architecture, shown in Figure 12, was deployed onto an LCW-based platform. The platform utilized Teflon AF tubing to simultaneously hold the biosensor solution, as well as confine and propagate the emitted fluorescence. In addition, the optical transparency of the tubing allowed illumination light to be launched transversely with respect to the tubing axis. By doing so, the amount of illumination light entering the detector is minimized, and only the fluorescent signal is gathered.

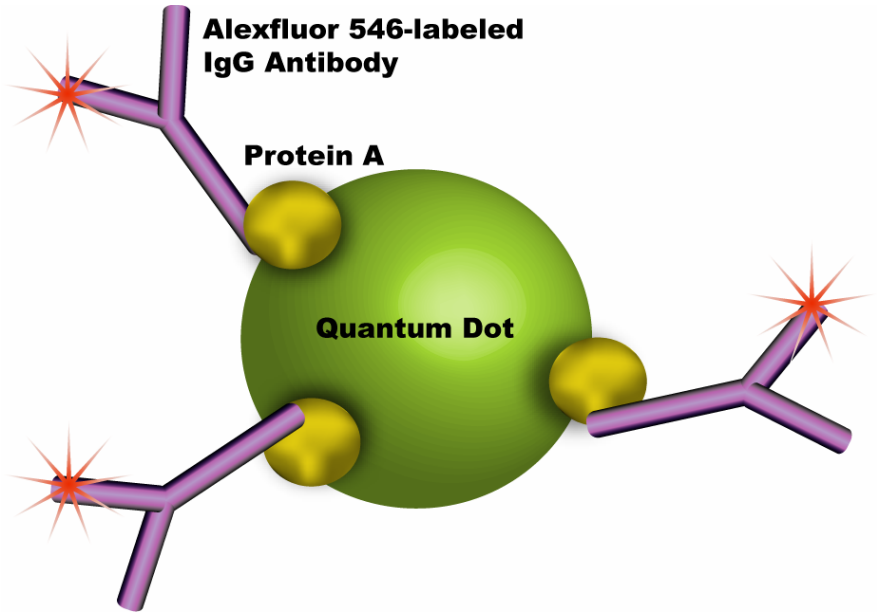

Figure 12. Schematic of the optical biosensor architecture

In order to test the proposed optical biosensor with the LCW platform, human cTnI was chosen as the analyte of interest. The detection of an alternative analyte from the previously described studies was carried out by only replacing the previous antibody in the biosensor complex with the appropriate analyte-specific antibody.

4.2 Materials and Methods

4.2.1Biosensor Fabrication

Labeling of biological macromolecules was conducted as previously described. Briefly, Protein A was labeled with Catskill green carboxyl-functionalized quantum dots. Mouse anti-Troponin I IgG monoclonal antibody was purchased from Fitzgerald Laboratories (Concord, MA) and labeled with Alexa-fluor 546.

After appropriate labeling of Protein A and anti-cTnI antibody, the biosensor complex was again fabricated by self-assembly. This was accomplished by combining the two reagents and incubating the solution for approximately 2 hours at room temperature.

In order for the largest changes in energy transfer to be induced, a proper acceptor to donor ratio must be used. The most effective ratio must allow both the donor and acceptor emission peaks to remain distinct and quantifiable. By qualitatively examining the emission peaks of the FRET pair in the biosensor solution, it was determined that a 4:1 Alexa-fluor 546 to quantum dot ratio provided the emission spectrum with noticeable peaks and measurable energy transfer changes. This FRET pair ratio was used for all subsequent experiments.

4.2.2 Waveguide Preparation

Teflon AF-2400 Tubing was purchased from Biogeneral, Inc (San Diego, CA), standard glass capillary tubes were purchased from Fisher Scientific (Waltham, MA), and polyimide-coated light guiding flexible fused silica capillary tubing was purchased from Polymicro Technologies (Phoenix, AZ). The Teflon AF tubing was cut into 5 cm segments with a scalpel, and the light guiding tubing was cut into 5 cm segments with a diamond scribe and then polished until each terminus was smooth and flat.

Fluorescein, a dye with fluorescence emission at a wavelength of approximately 514 nm, was purchased from Sigma-Aldrich (St. Louis, MO). The fluorescein was diluted to concentrations of 0.1, 1, and 10 μM in PBS. Loading of the fluorescein into the capillary tubes was accomplished by using a vacuum line to pull the solution through

the tube. For the Teflon AF tubes, one terminus of the tubing segment was fixed to a microsyringe so that the sample could be pulled into the tubing and then withdrawn so that the tubing segment could be reused after washing with distilled water. After loading of the fluorescein solution, the waveguide tubes were positioned onto a stage in which illumination was launched transversely with a Thorlabs blue-violet laser diode module (Newton, NJ) at a wavelength of 405 nm. For power study experiments comparing the three waveguide platforms, optical power was measured using a Newport 1930C optical power meter (Irvine, CA) at a wavelength of 518 nm. In addition to comparing the fluorescence transmission of the three platforms, the inter-tubing fluorescence transmission variation of the Teflon AF tubing was studied. For these experiments, the fluorescence emission was measured by coupling the LCW to an Ocean Optics 600 μm core diameter optical fiber and then into an Ocean Optics USB2000 miniature fiber optic spectrometer (Dunedin, FL) and finding the intensity of the fluorescence emission peak.

4.2.3 Biosensor Measurements

Once fabrication of the biosensor complex was complete, the solution was divided into 3.33 μl aliquots for use, and human cardiac Troponin I antigen (Scripps Laboratories) was added to the solution and incubated when appropriate. The solution was then brought to a total volume of 20 μl with phosphate buffered saline (PBS).

The sensor solution was drawn into 5 cm segments of Teflon AF with a microsyringe. The Teflon tube was positioned onto a stage with one terminus coupling into a 600-μm-core diameter optical fiber and clamped into place. The Teflon tube containing the biosensor solution was illuminated transversely with the blue-violet laser

diode module. At this wavelength, there is minimal direct excitation of the acceptor with the illumination source. Fluorescent emission of the FRET pair was propagated to the terminus of the Teflon tubing through the liquid core and coupled into the optical fiber. The biosensor emission was then directed to the fiber optic spectrometer via the optical fiber and a real-time fluorescence emission spectrum was obtained. Figure 13 displays an image of the stage used to take biosensor measurements with the Teflon AF tubing LCW biosensor.

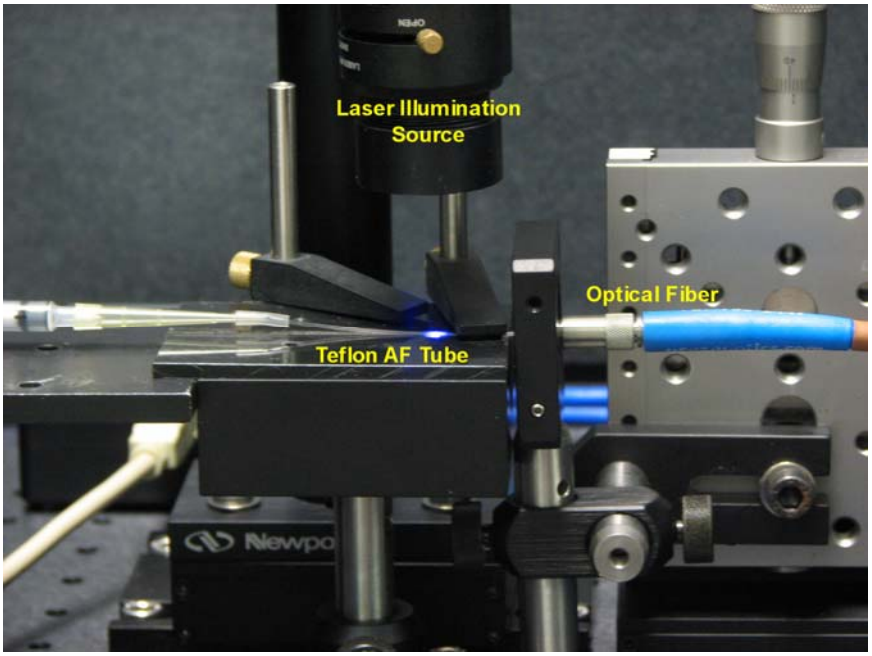

Figure 13. Image of biosensor platform stage

Biosensor response was quantified using the emission peaks of the donor and acceptor from the raw fluorescence spectrum. The peak value of the acceptor was divided by the peak value of the donor, yielding an acceptor to donor ratiometric biosensor value (A/D).

4.3 Results and Discussion

4.3.1 Waveguide Characterization

To ensure that the particular LCW platform would perform with high efficacy, the fluorescence light guiding properties of the Teflon-based LCW were characterized and compared to other light guiding methods. For comparison studies, the three waveguides being studied, standard capillaries, light guiding capillaries, and Teflon AF tubes, were loaded with 0, 0.1, and 1.0 μM fluorescein solution. The optical power output was measured and shown in Figure 14.

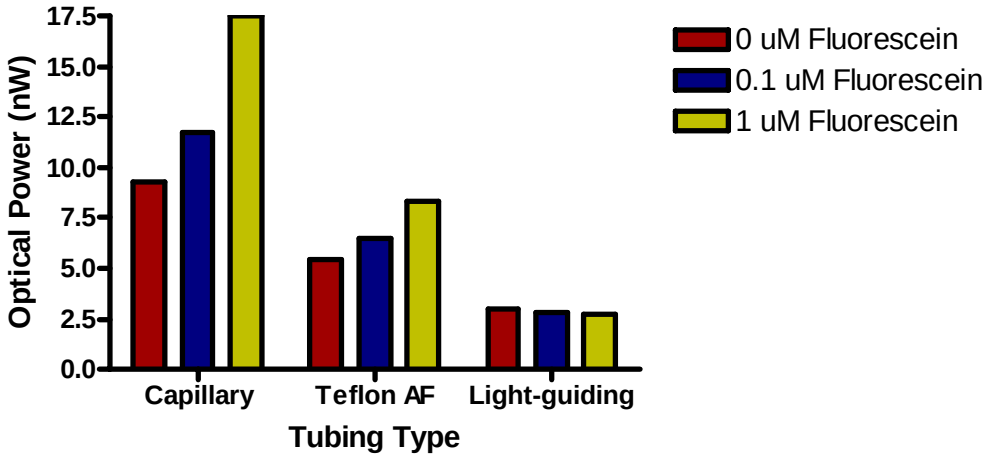

Figure 14. Fluorescence transmission for three waveguide tubing platforms

The results indicate that, due to the higher optical power reading compared to the control solution of 0 μM, the standard glass capillaries have a greater degree of fluorescence transmission. However, the inner diameter of the glass capillaries is approximately 1.1 mm, which is considerably larger than that of the Teflon AF tubing inner diameter of 0.8 mm. It can then be assumed that the higher signal observed in the standard glass capillaries occurred due to a larger volume of fluorescein solution being

illuminated. In addition, the increased background signal of the standard capillary tubes is a disadvantage for fluorescent biosensor applications. In the case of the light guiding capillaries, the doped silica outer cladding is surrounded by an opaque polyimide coating that minimizes the amount of illumination light allowed to enter the tubing transversely and so no fluorescence output is observed.

Although the Teflon tubing-based waveguide was compared to capillary tubing-based waveguides, the capillary-based waveguides are not true LCWs. Because the glass and silica that are used to hold the fluid have higher refractive indices than the fluid core, TIR does not occur in the fluid and instead fluorescence will travel within the glass and silica materials. The light is refracted into the tubing itself, and then interacts with the the next, outer interface and the liquid filled cavity. For standard glass capillaries, the outer interface is air, while for the light guiding capillaries, the outer interface is a doped silica. In both cases, the light interacts with a medium of lower refractive index than the one within which it is traveling and, if the angle of incident light is larger than the critical angle, TIR occurs. This confines the light within the tubing material itself and not the fluid core. Because Teflon AF is a true LCW system and has sufficient fluorescence transmission properties, it was chosen as the optimum biosensor platform.

Next, the inter-tubing variation between the Teflon AF tubes was examined. This ensures that the platform is capable of obtaining consistent measurements. In order to study the inter-tubing variation, three different Teflon AF tubing segments were chosen and loaded with fluorescein samples with concentrations of 0, 0.1, 1, and 10 μM. The peak fluorescence emission was measured and plotted over the logarithm of the fluorescein concentration used. These results are shown in Figure 15.

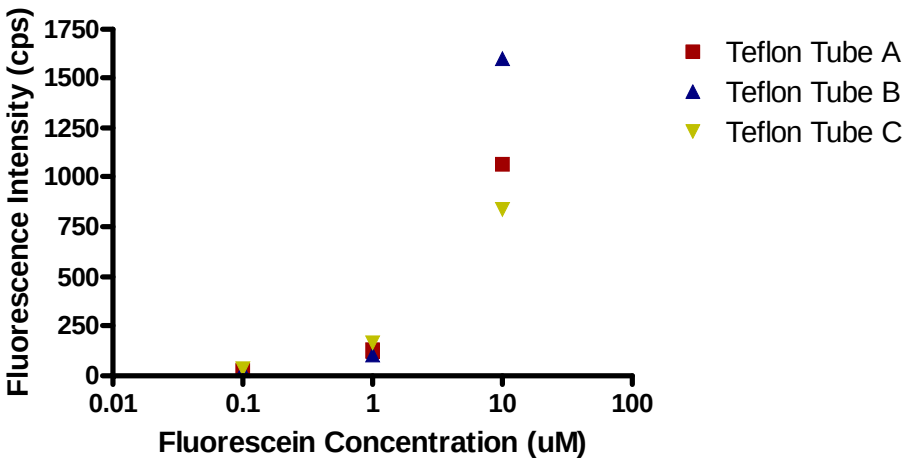

Figure 15. Inter-tubing variation for three Teflon AF tubing segments over a range of fluorescein concentrations

By examining the results, it can be assumed that minimal variation in fluorescence intensity occurs between 0 and 1 μM fluorescein concentrations. This indicates that each Teflon AF tubing segment has consistent transmission properties. Since the segments are cut from a single tube, this is to be expected. However, a relatively large amount of fluorescence intensity dispersion occurs at a concentration of 10 μM. Such a concentration of fluorescein is extremely large, and this degree of fluorescence emission will not occur with the proposed biosensor. Therefore, the optical properties of the Teflon-based LCW platform, particularly fluorescence transmission, are adequate to measure an acceptable degree of fluorescence emission, and this can also be performed with relative consistency.

4.3.2 Human cTnI Concentration Response

The response of the biosensor to various concentrations of cTnI was first examined. Biosensor solutions were exposed to concentrations of cTnI ranging from 0-1.745 μM. The upper limit of 1.745 μM is the theoretical saturation of the biosensor. As the concentration of cTnI antigen is increased, a greater number of sensor complexes undergo a conformational change and a larger change in A/D value occurs until the sensor reaches saturation. By plotting the derived A/D biosensor values versus the corresponding concentration of antigen added to the biosensor solution, a dose response curve is generated, as shown in Figure 16.

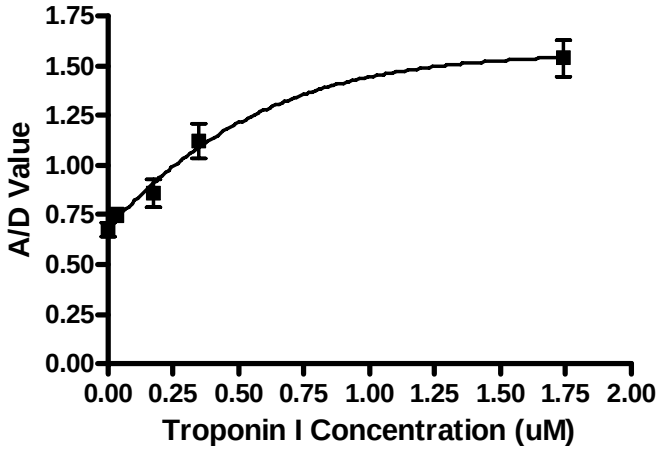

Figure 16. Dose response curve for human cTnI biosensor

The lower limit of detection of the biosensor was found to be approximately 32 nM. Saturation of the sensor is reached at around 500 nM, and the dose response curve shows a linear fit with high sensitivity over the antigen concentration range 32-500 nM. Also, with an R^2 value of 0.91, the predictive value of the sensor is satisfactory.

Although these results indicate that the proposed biosensor is a feasible method of human cTnI detection, they are still inferior to other methods that are currently available commercially. Such cTnI assays are capable of sub-nanomolar, and in some cases sub-picomolar detection. In addition, it is common for these systems to detect multiple analytes simultaneously.

4.3.3 Lower Limit of Detection

In an attempt to lower the limit of detection to a level similar to that of current and commercially available detection methods, the concentration range of cTnI exposed to the biosensor solution was drastically reduced. Lower limits of detection for these assays range from 0.01-0.1 ng/ml. To create an appropriate curve with a concentration range capable of achieving a limit of detection at or below 0.1 ng/ml, cTnI concentrations were varied from 0-50 ng/ml. The A/D values for each concentration measurement were found and these values were plotted to obtain the dose response curve shown in Figure 17.

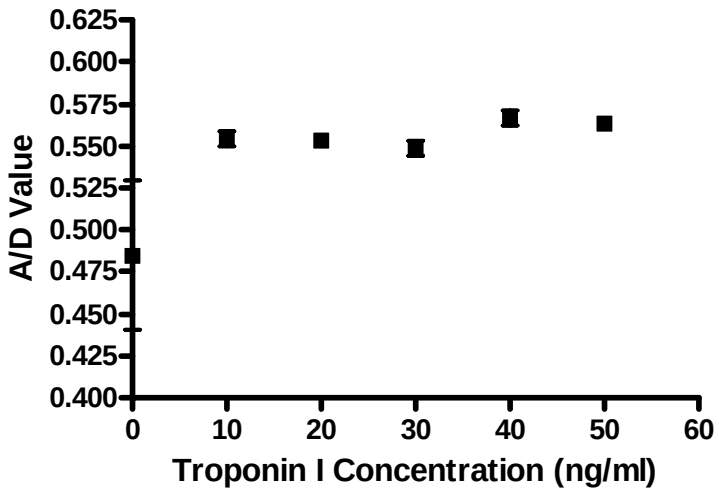

Figure 17. Dose response curve for lower limit of cTnI detection

Although there is a considerable difference in A/D biosensor value for the biosensor solutions exposed to cTnI when compared to that of the 0 ng/ml control, there is no discernible trend. The lack of linear trend within the working range of the sensor makes it difficult to derive a limit of detection for these experiments. It is worthy to note, however, that concentrations as small as 10 ng/ml are detectable with the biosensor technique. In addition, over the 3 repetitions of the experiment, the only variation in A/D biosensor value that occurred over the range of cTnI concentrations was the 0 ng/ml control. The large error in this concentration, however, occurred due to a single outlier. It is conceivable, then, that with further development, the biosensor could achieve a lower limit of detection comparable to that of the commercially available Troponin assays.

4.3.3 Biosensor Time Response

In order to determine the duration of antigen exposure required, the sensor solutions were exposed to a 1.745 μM concentration of cTnI antigen with varying incubation times. After addition of antigen, the biosensor solutions were incubated for durations ranging from 1-10 minutes. The incubation times include loading of the sensor solution into the Teflon AF tubing and placement into the stage for measurement. The curve depicting the time response of the biosensor is shown in Figure 18.

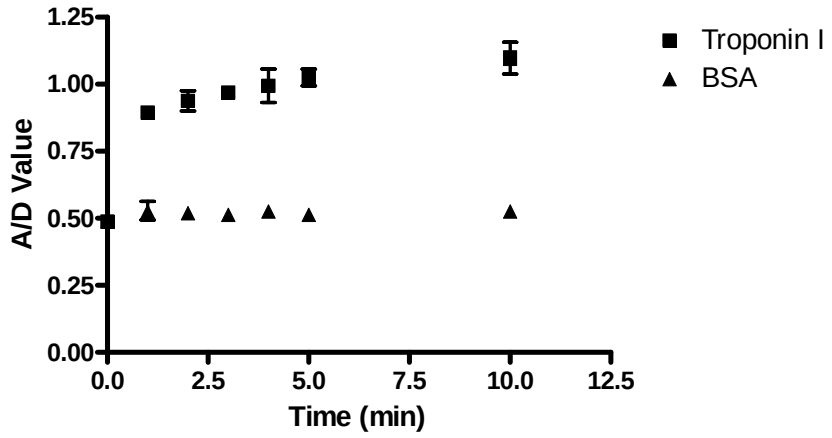

Figure 18. Time response for cTnI versus BSA

Although a small amount of antigen binding continues to occur afterward, the largest change in A/D biosensor value takes place within the first minute of antigen exposure. This is a relatively rapid binding reaction, but is not surprising when the high binding affinity of the antibody-antigen interaction is considered.

When compared to commercially available assays, time response within one minute is clearly superior to the total assay times of at least 15 minutes required for current methods. Considering that the one-minute incubation time includes sample loading and placement, the only additional time required for the biosensor to complete a

diagnostic assay is for calculation of the biosensor value and the subsequent determination of analyte concentration, which is negligible.

In addition, the time response for cTnI is compared to that of the nonspecific antigen, BSA. From these results, the highly specific nature of the biosensor is demonstrated. At an antigen exposure duration of 10 minutes, the percent change in A/D value from the zero minute control for cTnI is ~ 134%, whereas for the nonspecific BSA, the percent change is < 3%. Because of the relatively small change in biosensor value that is observed for the nonspecific antigen, it can be assumed that the presence of such species in a sample will cause very little interference with proper sensor function.

4.4 Conclusions

The results of this study show that the proposed optical biosensor is capable of highly specific and rapid antigen detection. Also, the sensor achieves a high sensitivity and relatively low detection limit. These properties make the sensor well suited for an array of potential applications. For the specific purpose of human cTnI detection, however, the detection limit is not low enough to compete with current assays that are commercially available. If the proposed biosensor is to reach such a high level of sensitivity, further development is needed. In particular, the sensor must be optimized for detection of sub-nanomolar detection. To accomplish this, the reagent concentration must be reduced in order to decrease the optical background signal. By using a biosensor solution that contains fewer binding sites, each antigen binding event will produce a more exaggerated response with respect to the fluorescence signal of unbound biosensor complexes. By decreasing the optical background signal, though, the total fluorescence

emission will be decreased, and the electronic background signal of the detector must also be decreased. This can only be accomplished by using a more sensitive spectrometer, which increases the cost of the biosensor system. As an added disadvantage, by decreasing the limit of detection in this manner, the saturation region will also be decreased, producing a more narrow working range of antigen concentrations. On the other hand, to detect an alternative antigen, only the monoclonal antibody need be replaced within the sensor complex. Although doing this may alter certain properties, the primary function of the sensor should remain largely unchanged.

By applying the optical biosensor to a LCW platform, the versatility of the sensor is capitalized upon. Firstly, when the sensor is utilized in the fluid core of an LCW, it may be used as an in-solution sensor, as described previously. By doing so, binding sites are not sterically hindered by a substrate, as is often the case for immobilized sensor systems. However, if it would be more beneficial to do so, the sensor complex could be fabricated on the interior surface of the LCW cladding. This would create a flow-through type sensor scheme, in which the antigen is flowed through the liquid core, where it would interact and bind to the immobilized biosensor complex on the cladding surface.

In general, the proposed optical biosensor shows promise as a diagnostic immunoassay technique. The response of the sensor is rapid and highly specific, and lacks many of the disadvantages and problems inherent in many other fluorescent optical biosensors. The use of antibody conformational changes within the biosensor complex in combination with the highly sensitive FRET technique, as well as the use of quantum dots as FRET donors, increases the efficacy of the sensor. Moreover, by applying the biosensor to a robust LCW platform, its overall performance is further enhanced.

CHAPTER 5. FABRICATION OF SILICON-BASED WAVEGUIDE DEVICES

5.1 Overview

For a field-deployable biosensor device to provide optimum functionality, it must be relatively small. This gives the device portability, making it practical for a large range of environments and conditions. In a clinical setting, for example, a smaller diagnostic device uses less valuable bench top space. Alternatively, for environmental diagnostics, where the device must be carried over long distances, a more compact, energy efficient, and lightweight design increases the ease of use. By this convention, then, a biosensor device would be most applicable if it were as small as possible.

A silicon substrate-based microchip platform would decrease the size used in an optical device and also produce other advantages. These advantages include the deployment of integrated optics components, which would allow the entire device to function in a small space all on one chip. Also, for LCW devices, the advent of microfluidics and microelectromechanical systems (MEMS) gives the device the ability to use extremely small volumes of fluid with compact components in a highly automated manner.

The first step in the realization of such a device being applied to the proposed optical biosensor is the study and deployment of the appropriate LCW platform. The platform should be silicon substrate-based, but still allow the biosensor to function properly. Additionally, the platform should use minimal volumes of fluid while still producing useable optical signals, or as in this case, fluorescent transmission. The

platform should also allow the integration of micro- and nano-optical components, as well as microfluidic and MEMS components.

5.2 Materials and Methods

5.2.1 Etching of Microchannels in Silicon

Silicon substrates were pre-prepared by deposition of a 200 nm silicon carbide layer followed by deposition of a 300-400 nm layer of aluminum, with the silicon carbide acting as the hard mask for silicon etching and the aluminum acting as the etch mask for silicon carbide etching. These substrates were then fractioned into 1-inch square wafers. Channels were patterned onto the substrate using conventional photolithographic techniques. Essentially, a photoresist layer was spin coated onto the outer aluminum surface and then baked at 90^{o}C for approximately 10 minutes. A negative photomask was used create channels of 200 μm and 400 μm widths by exposing portions of the substrate that were not to be etched away to an intense ultraviolet light source. The exposed portions of photoresist become cross-linked, making them more chemically robust. After exposure, the substrate was again baked at 90^{o}C for 10 approximately 10 minutes and then developed to remove unexposed portions of the photoresist, leaving the substrate ready to be etched.

The portions of aluminum not covered by the cross-linked photoresist were etched away using an aluminum etchant that consists of phosphoric acid, acetic acid, nitric acid, and distilled water. The substrate was immersed in the etchant solution until the exposed aluminum dissolved, producing the aluminum etch mask for silicon carbide etching.

Silicon carbide was then plasma etched for 320 minutes, and the remaining aluminum etch mask was then removed by an additional exposure to the aluminum etchant.

Microchannels in the silicon wafer were then etched using the silicon carbide hard mask. A 75% solution of potassium hydroxide was dissolved in 15 ml distilled water at 225^{o}C with constant stirring. Once a clear solution was obtained, the temperature was reduced to 150^{o}C and approximately 0.025 g antimony trioxide was added to the mixture. With continued stirring, the substrate was immersed into the resulting etchant solution at 120^{o}C. The etch rate was considered to be 1.3-1.4 μm/min, and so a exposure duration of approximately 45 minutes was used to obtain channels in the silicon wafer with a depth of around 60 μm. All remaining silicon carbide was then removed by plasma etching, leaving only the patterned silicon wafer.

5.2.2 Fabrication of Waveguide Device

After microchannels were etched into the silicon substrates, the LCW device could be fabricated. To do so, borosilicate glass was cut into sections with a width equal to and a length slightly less than the patterned silicon wafer. Both the glass and silicon substrates were washed with a series of organic solvents. The substrates were then treated with an adhesion layer to allow the attachment of the Teflon cladding to the substrate. The adhesion substance, FSM 660, was purchased from Cytonix Corporation (Beltsville, MD) and spin coated onto the substrates at a spin speed of 3500 rpm for 30 seconds. Following a bake at 90^{o}C for 10 minutes, each substrate was left with a monolayer of fluoroalkyl monosilane bonds.

Teflon AF-1600 in-solution resin was purchased from DuPont (Wilmington, DE) and deposited onto the substrate surfaces by spin coating at a spin speed of 3000 rpm for 30 seconds. At this spin speed and duration, a Teflon AF layer of approximately 4 μm was produced. Next, the substrates were baked at 90°C for 15 minutes, 165°C for 15 minutes, 245°C for 15 minutes, and then 330°C for 30 minutes, consecutively. This annealing process vaporizes the Teflon AF solvent and creates a smooth, homogeneous Teflon cladding layer. With a face of each substrate coated in a thin layer of Teflon AF, they were then clamped together with the Teflon-coated surfaces facing inward and baked at 330°C for 30 minutes. At this temperature, the annealing process facilitates thermal bonding of the Teflon-coated surfaces that are in contact. The result is a sealed microchannel coated with a thin, transparent cladding of Teflon AF 1600, the cross-section of which is depicted in Figure 19.

Figure 19. Cross-section diagram of silicon substrate-based LCW device

5.3 Results and Discussion

Using the microfabrication and assembly procedures detailed previously, four waveguide devices were fabricated. Two of the devices contained three microchannels with a width of 400 μm. The other two devices, one of which is shown in Figure 20,

contained four microchannels with a width of 400 μm and four microchannels with a width of 200 μm.

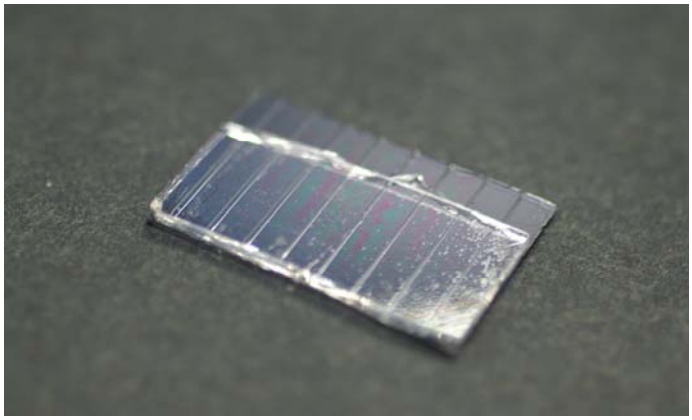

Figure 20. Image of completed silicon substrate-based LCW device

Although the devices appear to have been fabricated properly, characterization of the optical properties of the fluid-filled microchannels was not accomplished. The Teflon AF cladding is extremely hydrophobic. Due to the hydrophobicity of the cladding along with the relatively small size of the channels, aqueous samples could not be introduced to either terminus of the channels using a micropipette or microsyringe. However, it has been shown that a 0.75 mm hole drilled through the borosilicate glass substrate and then aligned with the etched silicon channel during annealing allows fluid to be injected into the channel with a micropipette, assuming that the micropipette tip fits firmly into the 0.75 mm hole, allowing enough pressure to be applied. This is likely the only way that fluid can be introduced into the device using basic pipetting or injection methods. As an alternative to the tedious procedure of aligning the two substrates so that the 0.75 mm hole directly overlaps the etched silicon channel, a permanent coupling method could be utilized. The envisioned method would include the permanent fixture of a length of

tubing to one of the microchannel termini, likely with a UV-curable epoxy or similar technique. The opposite end of the tubing could then be fitted around a syringe needle or micropipette tip for easy loading. Also, loading of fluidic samples would conceivably be easier with a wider and deeper channel, although smooth, homogeneous surfaces are difficult to attain with microchannels of this size.

5.4 Conclusions

Even though the silicon substrate-based microchannel LCW devices are a promising platform for deployment of optical biosensors, they have certain inherent disadvantages. First and foremost is the difficulty of introducing fluidic samples into the devices, though as mentioned previously, there are ways of alleviating these problems. Secondly, the microchannels hold such small volumes of fluid that it may be difficult to obtain measurable fluorescence signals from their termini. This problem is compounded by the additional complication of the device's inability to allow illumination light to pass through the waveguide transversely. Since one side of the channel is transparent, illumination light may enter through that surface. However, instead of being transmitted out of the waveguide through the adjacent surface, it interacts with the silicon that the surface is comprised of. The channels are fabricated in such a way that the silicon surfaces are smooth and mirror-like, so that light is reflected back out of the waveguide, but a degree of dispersion occurs nonetheless. This dispersion increases the optical background of the platform, which acts as an added disadvantage.

Generally, the Teflon AF tubing is a highly effective method for launching the proposed LCW platform, and has no major disadvantages or shortcomings when

compared to the substrate-based microchannel devices. The tubing-based platform uses sufficiently small volumes for most of the foreseeable optical biosensor applications and functions quite well for such applications. Also, the fabrication of the substrate-based devices is time-consuming and expensive, whereas the Teflon AF tubing can be purchased for a reasonable price, and upon receipt, only has to be segmented into the desired lengths and is then ready to use. Therefore, the silicon chip LCW platform has been tentatively, and perhaps permanently, abandoned for deployment of the proposed fluorescent optical biosensor.

CHAPTER 6. FUTURE WORK

As a first step in continued sensor development, the optical biosensor could be further optimized in order to increase its response sensitivity and accuracy. The easiest way of accomplishing this would be to continue to examine the optimal reagent ratios along with the concentration of biosensor complex in solution. Although reagent ratios have been examined, it is an approximate ratio that provides a large response. The truly optimal reagent ratio could potentially vary slightly from the ratio used in these studies. Of greater importance is the optimum concentration of biosensor complex in the sensor solution. Altering the biosensor complex concentration changes the function of the sensor in several different ways. By increasing the concentration, for instance, a higher fluorescence background signal will be produced and so the sensor will be less sensitive to smaller concentrations of analyte, but at the same time, the concentration of analyte at which the sensor becomes saturated will increase, generating a wider working range. On the other hand, by decreasing the biosensor complex concentration, the sensitivity to small concentrations of analyte will be increased, while the detectable fluorescence signal will be decreased. In this manner, the biosensor complex concentration will reach a point at which it will no longer be measurable by the detector device.

Another method of optimizing the proposed biosensor would be to study the effect of different FRET pairs. Because of their size-tunability, quantum dots can be purchased with a variety of different emission wavelengths, and a huge array of traditional organic fluorescent dyes is also available to be produced or purchased to create a viable FRET dye pair. Therefore, the number of possible FRET pairs is quite

extensive. The Catskill green quantum dot/Alexafluor 546 pair utilized in this study worked very effectively, but it is conceivable that other pairs of fluorophores exist that could carry out the task with a higher degree of efficacy.

One aspect that must be addressed in a more complete way is the amendment of the biosensor architecture to detect different analytes. It has been shown during the course of this study that the sensor can be effectively used to detect PRRSV and human cTnI, but continued studies should be used to show that the sensor is able detect many different analytes with high effectiveness by simply replacing the IgG antibody within the biosensor complex. As an added study, the use of polyclonal antibodies rather than monoclonal antibodies could also be studied. By using polyclonal antibodies, a range of related analytes could potentially be detected. This would be particularly useful for detection of highly adaptable viral antigens. Using polyclonal antibodies, multiple strains of the same virus could be detected instead of one single strain, making the biosensor more capable and robust.

In conjunction with further development of the nano-biosensor architecture, the platform to which the sensor is applied could also be improved. One obvious method of expanding the study of biosensor platforms would be to examine other LCW devices. Alternatives to the Teflon AF-2400 tubes that were successfully utilized are capillary tubes with an inner Teflon AF cladding and, as described previously, silicon substrate-based microchannels with Teflon AF inner claddings. In addition, the advent of nano-porous silica-based cladding materials could provide an option to the proprietary Teflon AF cladding material. In particular, Teflon's extremely hydrophobic and nonstick properties make it difficult to immobilize biological macromolecules or functional groups

to the surface for immobilization techniques. Nano-porous silica materials, on the other hand, produce a substrate that could be functionalized for immobilization of the biosensor complex. By immobilizing the biosensor complex, it is likely that some antigen binding functionality may be lost, but it is also possible that the effectiveness of the sensor could be increased. Additionally, the biosensor could be used in a sample flow-through type of configuration.

Once the optical biosensor architecture and sensor platform have been sufficiently optimized, the biosensor can be deployed for use in field diagnostics. Even in the current bench top system that was utilized in the study, most of the components used to gather data were relatively small. These components include the laser module, Teflon tubing stage, handheld spectrometer, and laptop computer for user interfacing. In order to further decrease the size of the individual components, the laser module could be replaced with a light emitting diode (LED) illumination source and the laptop could be replaced with a micro-controller and digital display. Once this type of system is in use, the components could be condensed into one single device. Considering the small size of all of these components and the ways in which they could be arranged, the envisioned device could feasibly be a lightweight handheld unit. In order to be cost efficient, this device would likely utilize a measurement system that could be coupled with a disposable cartridge that would contain the sample input, LCW platform, and LED illumination source. Once the measurement was taken, the cartridge could be disposed of and a new one used for the next measurement.

This proposed device could be deployed for a number of detection purposes, ranging from water contamination to medical diagnostics. The lightweight and compact

nature of the device would enable it to be used in a variety of environments. Also, the potential low cost of the device would allow it to be accessible for many resource-limited settings. In general, the envisioned biosensor device could be highly commercially viable, and capable of competing with a host currently used diagnostic methods, as well as filling unoccupied diagnostic technique niches.

REFERENCES

1. Eggins, B. R. 2002. *Chemical Sensors and Biosensors*, Chichester, England: John Wiley & Sons.

2. Brecht, A. and Gauglitz, G. 1995. Optical Probes and Transducers. *Biosensors and Bioelectronics* 10: 923-936.

3. Lechuga, L. M. 2005. *Biosensors and Modern Biospecific Analytical Techniques*, ed. Gordon, L. Comprehensive Analytical Chemistry, Amsterdam: Elsevier B.V.

4. Lakey, J. H. and Raggett, E. M. 1998. Measuring Protein--Protein Interactions. *Current Opinion in Structural Biology* 8(1): 119-123.

5. Lakowics, J. R. 1999. *Principles of Fluorescence Spectroscopy*, 2nd Ed., New York: Kluwer Academic/Plenum Publishers.

6. Yang, X., Zhou, Z., Xiao, D., and Choi, M. M. F. 2006. A Fluorescent Glucose Biosensor Based on Immobilized Glucose Oxidase on Bamboo Inner Shell Membrane. *Biosensors and Bioelectronics* 21(8): 1613-1620.

7. Rowe-Taitt, C. A., Golden, J. P., Feldstein, M. J., Cras, J. J., Hoffman, K. E., and Ligler, F. S. 2000. Array Biosensor for Detection of Biohazards. *Biosensors and Bioelectronics* 14(10-11): 785-794.

8. Berdat, D., Marin, A., Herrera, F., and Gijs, M. A. M. 2006. DNA Biosensor Using Fluorescence Microscopy and Impedance Spectroscopy. *Sensors and Actuators B: Chemical* 118(1-2): 53-59.

9. Clegg, R. M. 1996. *Fluorescence Imaging Spectroscopy and Microscopy*, ed. Wang, X. F. and Herman, B., vol. 137, New York: John Wiley & Sons, Inc.

10. Grant, S. A., Xu, J., Bergeron, E. J., and Mroz, J. 2001. Development of Dual Receptor Biosensors: An Analysis of FRET Pairs. *Biosensors and Bioelectronics* 16: 231-237.

11. Hsu, Y. Y., Liu, Y. N., Wang, W., Kao, F. J., and Kung, S. H. 2007. In Vivo Dynamics of Enterovirus Protease Revealed by Fluorescence Resonance Emission Transfer (FRET) Based on a Novel FRET Pair. *Biochemical and Biophysical Research Communications* 353(4): 939-945.

12. Ko, S. and Grant, S. A. 2006. A Novel FRET-Based Optical Fiber Biosensor for Rapid Detection of Salmonella Typhimurium. *Biosensors and Bioelectronics* 21(7): 1283-1290.

13. Prasad, P. N. 2004. *Nanophotonics*, Hoboken, NJ: John Wiley & Sons, Inc.

14. Link, S. and El-Sayed, M. A. 2000. Shape and Size Dependence of Radiative, Non-Radiative and Photothermal Properties of Gold Nanocrystals. *International Reviews in Physical Chemistry* 19(3): 409-453.

15. Dulkeith, E., Morteani, A. C., Niedereichholz, T., Klar, T. A., Feldmann, J., Levi, S. A., van Veggel, F. C. J. M., Reinhoudt, D. N., Moller, M., and Gittins, D. I. 2002. Fluorescence Quenching of Dye Molecules Near Gold Nanoparticles: Radiative and Nonradiative Effects. *The American Physical Society* 89(20): 1-4.

16. Lochner, N., Lobmaier, C., Wirth, M., Leitner, A., Pittner, F., and Gabor, F. 2003. Silver Nanoparticle Enhanced Immunoassays: One Step Real Time Kinetic Assay for Insulin Serum. *European Journal of Pharmaceutics and Biopharmaceutics* 56: 469-477.

17. Simonian, A. L., Good, T. A., Wang, S.-S., and Wild, J. R. 2005. Nanoparticle-Based Optical Biosensors for the Direct Detection of Organophosphate Chemical Warfare Agents and Pesticides. *Analytica Chimica Acta* 534: 69-77.

18. Wu, Z.-S., Jiang, J.-H., Fu, L., Shen, G.-L., and Yu, R.-Q. 2006. Optical Detection of DNA Hybridization Based on Fluorescence Quenching of Tagged Oligonucleotide Probes By Gold Nanoparticles. *Analytical Biochemistry* 353: 22-29.

19. Azzazy, H. M. E., Mansour, M. M. H., and Kazmierczak, S. C. 2006. Nanodiagnostics: A New Frontier for Clinical Laboratory Medicine. *Clinical Chemistry* 52(7): 1238-1246.

20. Michalet, X., Pinaud, F. F., Bentolila, L. A., Tsay, J. M., Doose, S., Li, J. J., Sundaresan, G., Wu, A. M., Gambhir, S. S., and Weiss, S. 2005. Quantum Dots for Live Cells, in Vivo Imaging, and Diagnostics. *Science* 307(5709): 538-544.

21. Medintz, I. L., Uyeda, H. T., Goldman, E. R., and Mattoussi, H. 2005. Quantum Dot Bioconjugates for Imaging, Labelling and Sensing. *Nature Materials* 4: 435-446.

22. Medintz, I. L., Clapp, A. R., Mattoussi, H., Goldman, E. R., Fisher, B., and Mauro, M. J. 2003. Self-Assembled Nanoscale Biosensors Based on Quantum Dot FRET Donors. *Nature Materials* 2: 630-638.

23. Nikiforov, T. T. and Beechem, J. M. 2006. Development of Homogeneous Binding Assays Based on Fluorescence Resonance Energy Transfer Between Quantum Dots and Alexa Fluor Fluorophores. *Analytical Biochemistry* 357: 68-76.

24. Medintz, I. L., Clapp, A. R., Brunel, F. M., Tiefenbrunn, T., Uyeda, H. T., Chang, E. L., Deschaps, J. R., Dawson, P. E., and Mattoussi, H. 2006. Proteolytic Activity Monitored by Fluorescence Resonance Energy Transfer Through Quantum-Dot-Peptide Conjugates. *Nature Materials* 5: 581-589.

25. Killard, A. J., Deasy, B., O'Kennedy, R., and Smyth, M. R. 1995. Antibodies: Production, Functions and Applications in Biosensors. *Trends in Analytical Chemistry* 14(6): 257-266.

26. Widmaier, E. P., Raff, H., and Strang, K. T. 2004. *Human Physiology: The Mechanics of Body Function*, Ninth Ed., New York: McGraw-Hill.

27. Bongini, L., Fanelli, D., Piazza, F., De Los Rios, P., Sandin, S., and Skoglund, U. 2005. Dynamics of Antibodies From Cryo-Electron Tomography. *Biophysical Chemistry* 115: 235-240.

28. Lichlyter, D. J., Grant, S. A., and Soykan, O. 2003. Development of a Novel FRET Immunosensor Technique. *Biosensors and Bioelectronics* 19: 219-226.

29. Grant, S. A., Heits, B., and Kleiboeker, S. 2006. Development of an Optical Biosensor Utilizing Gold Nanoparticles to Detect Porcine Reproductive and Respiratory Syndrome Virus. *Sensor Letters* 4: 1-7.

30. Saleh, B. E. A. and Teich, M. C. 1991. *Fundamentals of Photonics* Wiley Series in Pure and Applied Optics, New York: John Wiley & Sons, Inc.

31. Okamoto, K. 2006. *Fundamentals of Optical Waveguides*, 2nd Ed., Burlington, MA: Elsevier Inc.

32. Teflon AF Amorphous Fluoropolymers. 1998. Wilmington, DE, DuPont Fluoroproducts.

33. Altkorn, R., Koev, I., Van Duyne, R. P., and Litorja, M. 1997. Low-Loss Liquid-Core Optical Fiber for Low-Refractive-Index Liquids: Fabrication, Characterization, and Application in Raman Spectroscopy. *Applied Optics* 36(34): 8992-8998.

34. Altkorn, R., Koev, I., and Pelletier, M. J. 1999. Raman Performance Characteristics of Teflon-AF 2400 Liquid-Core Optical-Fiber Sample Cells. *Applied Spectroscopy* 53(10): 1169-1176.

35. Holtz, M., Dasgupta, P. K., and Zhang, G. 1999. Small-Volume Raman Spectroscopy With a Liquid Core Waveguide. *Analytical Chemistry* 71(14): 2934-2938.

36. Dasgupta, P. K., Genfa, Z., Poruthoor, S. K., Caldwell, S., and Dong, S. 1998. High-Sensitivity Gas Sensors Based on Gas-Permeable Liquid Core Waveguides and Long-Path Absorbance Detection. *Analytical Chemistry* 70: 4661-4669.

37. Dasgupta, P. K., Genfa, Z., Li, J., Boring, B., Jambunathan, S., and Al-Horr, R. 1999. Luminescence Detection With a Liquid Core Waveguide. *Analytical Chemistry* 71(7): 1400-1407.

38. Li, J., Dasgupta, P. K., and Genfa, Z. 1999. Transversely Illuminated Liquid Core Waveguide Based Fluorescence Detection: Fluorometric Flow Injection Determination of Aqueous Ammonium/Ammonia. *Talanta* 50(3): 617-623.

39. Hanning, A., Lindberg, P., Westberg, J., and Roeraade, J. 2006. Laser-Induced Fluorescence Detection by Liquid Core Waveguiding Applied to DNA Sequencing by Capillary Electrophoresis. *Analytical Chemistry* 72(15): 3423-3430.

40. Wang, S.-L., Huang, X.-J., Fang, Z.-L., and Dasgupta, P. K. 2006. A Miniaturized Liquid Core Waveguide-Capillary Electrophoresis System With Flow Injection Sample Introduction and Fluorometric Detection Using Light-Emitting Diodes. *Analytical Chemistry* 73(18): 4545-4549.

41. Manor, R., Datta, A., Ahmad, I., Holtz, M., Gangopadhyay, S., and Dallas, T. 2003. Microfabrication and Characterization of Liquid Core Waveguide Glass Channels Coated With Teflon AF. *IEEE Sensors Journal* 3(6): 687-692.

42. Dallas, T. and Dasgupta, P. K. 2004. Light at the End of the Tunnel: Recent Analytical Applications of Liquid-Core Waveguides. *Trends in Analytical Chemistry* 23(5): 385-392.

43. Hanada, K., Suzuki, Y., Nakane, T., Hirose, O., and Gojobori, T. 2005. The Origin and Evolution of Porcine Reproductive and Respiratory Syndrome Viruses. *Molecular Biology & Evolution* 22(4): 1024-1031.

44. Albina, E. 1997. Epidemiology of Porcine Reproductive and Respiratory Syndrome (PRRS): An Overview. *Veterinary Microbiology* 55: 309-316.

45. Cho, J. G. and Dee, S. A. 2006. Porcine Reproductive and Respiratory Syndrome Virus. *Theriogenology* 66: 655-662.

46. Botner, A. 1997. Diagnosis of PRRS. *Veterinary Microbiology* 55: 295-301.

47. Burness, C. E., Beacock, D., and Channer, K. S. 2005. Pitfalls and Problems of Relying on Serum Troponin. *QJ Med* 98: 365-471.

48. Babuin, L. and Jaffe, A. S. 2005. Troponin: The Biomarker of Choice for the Detection of Cardiac Injury. *Canadian Medical Association Journal* 173(10): 1191-1202.